Article

Immunity

Lipid-Droplet Formation Drives Pathogenic Group 2 Innate Lymphoid Cells in Airway Inflammation

Graphical Abstract

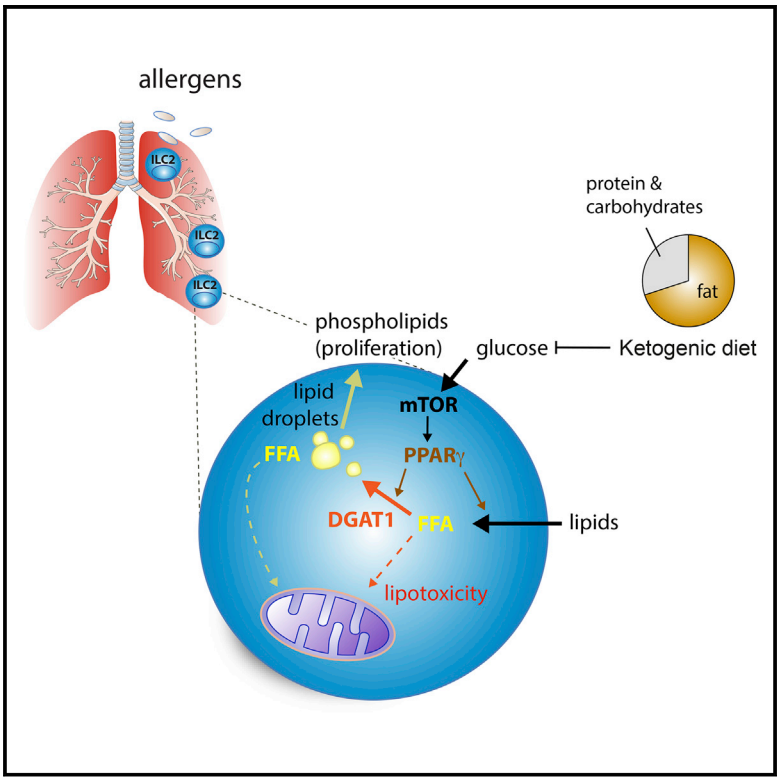

Highlights

- ILC2s take up external lipids, which are transiently stored in lipid droplets
- External lipids are converted into phospholipids to promote the proliferation of ILC2s
- PPARγ and DGAT1 control lipid uptake and transient storage in lipid droplets
- Ketogenic diet prevents ILC2-driven airway inflammation

Authors

Fotios Karagiannis,
Schekufe Kharabi Masouleh,
Klaus Wunderling, ..., Michael Hölzel,
Christoph Thiele, Christoph Wilhelm

Correspondence

christoph.wilhelm@uni-bonn.de

In Brief

Type 2 innate lymphoid cells (ILC2s) are contributing to the development of airway inflammation upon chronic activation. Karagiannis and colleagues reveal that external lipids transiently stored in lipid droplets are required to fuel pathogenic ILC2 responses and identify a ketogenic diet as a potent intervention strategy to treat ILC2-driven airway inflammation.

Karagiannis et al., 2020, Immunity *52*, 620–634
April 14, 2020 © 2020 Elsevier Inc.
https://doi.org/10.1016/j.immuni.2020.03.003

CellPress

CellPress

Immunity
Article

Lipid-Droplet Formation Drives Pathogenic Group 2 Innate Lymphoid Cells in Airway Inflammation

Fotios Karagiannis,[1,4] Schekufe Kharabi Masouleh,[1,4] Klaus Wunderling,[3] Jayagopi Surendar,[1] Vanessa Schmitt,[1] Alexander Kazakov,[1] Marcel Michla,[1] Michael Hölzel,[2] Christoph Thiele,[3] and Christoph Wilhelm[1,5,*]
[1]Immunopathology Unit, Institute of Clinical Chemistry and Clinical Pharmacology, Medical Faculty, University Hospital Bonn, University of Bonn, 53127 Bonn, Germany
[2]Institute of Experimental Oncology, Medical Faculty, University of Bonn, 53127 Bonn, Germany
[3]Life & Medical Sciences Institute (LIMES), University of Bonn, 53115 Bonn, Germany
[4]These authors contributed equally
[5]Lead Contact
*Correspondence: christoph.wilhelm@uni-bonn.de
https://doi.org/10.1016/j.immuni.2020.03.003

SUMMARY

Innate lymphoid cells (ILCs) play an important role in the control and maintenance of barrier immunity. However, chronic activation of ILCs results in immune-mediated pathology. Here, we show that tissue-resident type 2 ILCs (ILC2s) display a distinct metabolic signature upon chronic activation. In the context of allergen-driven airway inflammation, ILC2s increase their uptake of both external lipids and glucose. Externally acquired fatty acids are transiently stored in lipid droplets and converted into phospholipids to promote the proliferation of ILC2s. This metabolic program is imprinted by interleukin-33 (IL-33) and regulated by the genes *Pparg* and *Dgat1*, which are both controlled by glucose availability and mTOR signaling. Restricting dietary glucose by feeding mice a ketogenic diet largely ablated ILC2-mediated airway inflammation by impairing fatty acid metabolism and the formation of lipid droplets. Together, these results reveal that pathogenic ILC2 responses require lipid metabolism and identify ketogenic diet as a potent intervention strategy to treat airway inflammation.

INTRODUCTION

A prevailing health issue in industrialized countries is the increasing incidence of allergies and asthma, characterized by chronic inflammation of the airways (Bach, 2002). Asthmatic airway inflammation is a multifactorial condition that is characterized by hyperreactivity to external stimuli leading to inflammation, increased mucus production, obstruction, and fibrosis of the airways (Anderson, 2008; Fanta, 2009). The etiology of asthma is poorly understood, but one hypothesis is that factors related to a modern lifestyle, such as increased nutrient uptake and hygiene, may substantially influence disease incidence (Platts-Mills, 2015). As urbanization and industrialization continue to rise, chronic airway inflammation has developed into a major threat to public health in the Western world. This necessitates a better understanding of the causes leading to pathology and disease development.

Historically, asthma has been associated with allergen-specific $CD4^+$ T cells of the T helper-2 (Th2) compartment, which are found together with elevated numbers of eosinophils in the airways of asthmatic patients (Holgate and Polosa, 2008; Lloyd and Hessel, 2010; Robinson et al., 1992). More recently, type 2 innate lymphoid cells (ILC2s) have been identified as key players driving asthma through the production of cytokines such as interleukin-13 (IL-13) and IL-5 and the recruitment of eosinophils (Artis and Spits, 2015; Hammad and Lambrecht, 2015; McKenzie et al., 2014).

Mice and humans harbor three discrete ILC subsets (ILC1, ILC2, and ILC3) (Spits et al., 2013; Spits and Di Santo, 2011). ILCs play a major role in immunological defense and tissue maintenance at barrier sites. ILC2s are important for the repair of epithelial damage caused by tissue dwelling parasites and protection of the host against helminth infections (Artis and Spits, 2015). Such protective functions are mediated by the transcription factor GATA-3 and the coordinated production of the cytokines IL-5, IL-9, IL-13, and amphiregulin (Artis and Spits, 2015). However, chronic activation of ILC2s can cause allergen-induced airway inflammation by increasing mucus production and eosinophil recruitment to the airways (Artis and Spits, 2015; McKenzie et al., 2014; Spits et al., 2013). Unraveling the basic mechanisms underlying chronic ILC2 activation is therefore necessary for a better understanding of asthma development. In particular, identifying the metabolic requirements of ILC2-mediated pathology offers the unique opportunity to reveal how increased nutrient availability may contribute to disease development in the Western world. Simultaneously, knowledge about specific nutrients that drive disease could enable the use of dietary intervention as a cost-effective treatment for allergen-induced airway inflammation.

The study of metabolic programs fueling inflammation has largely focused on glycolysis as a major driver of immune cell activation. In activated immune cells, intermediates of glycolysis provide building blocks for anabolic processes. These processes include lipid, amino acid, and nucleotide synthesis and are required for proliferation and cytokine production in immune cells (Buck et al., 2015; Pearce and Pearce, 2013). Yet, to

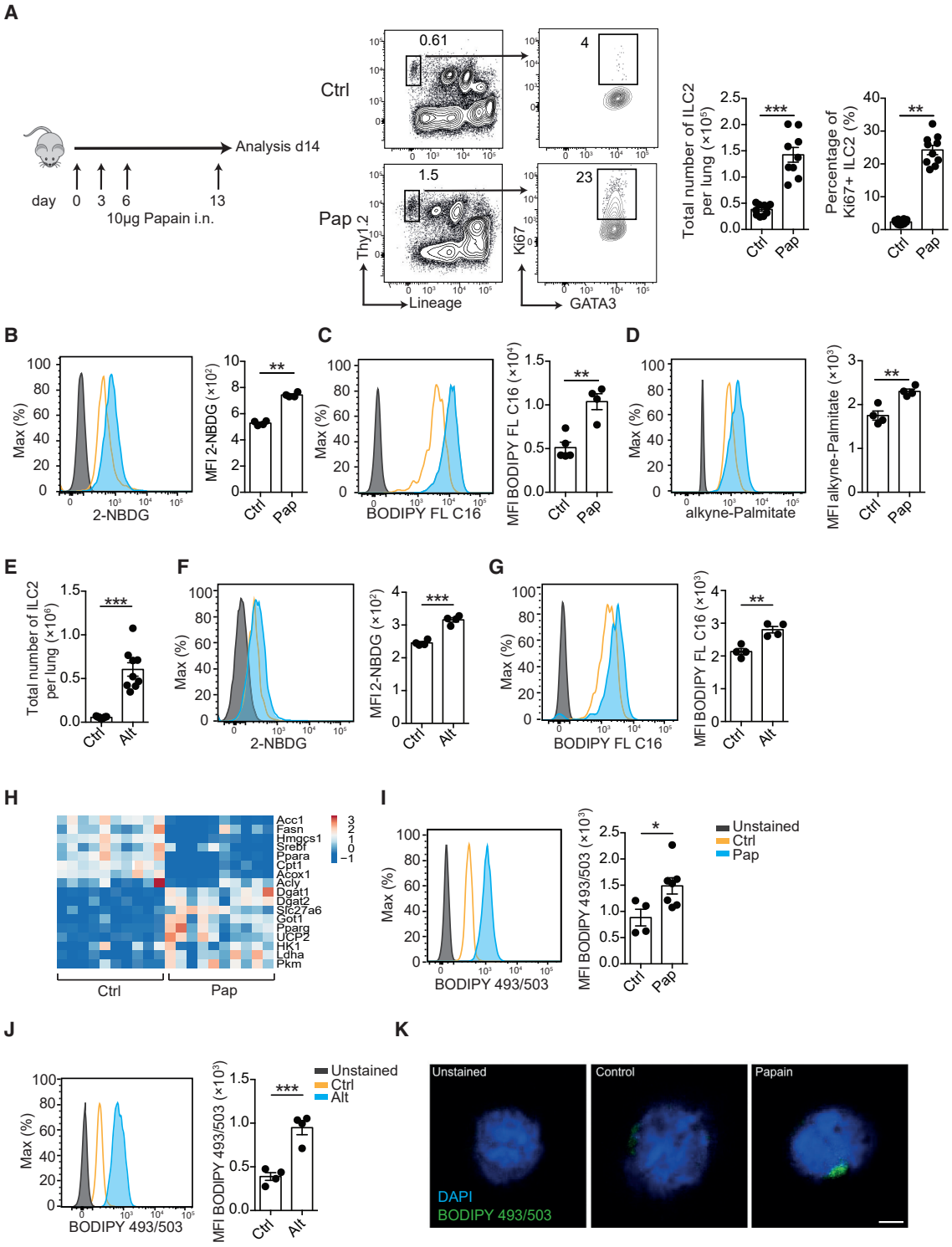

Figure 1. Chronic Activation Induces LD Formation in Pulmonary ILC2s

(A) Experimental schematic and gating strategy for ILC2s in the lung. C57BL/6 mice were challenged intranasally with PBS (Ctrl), papain (Pap), or *A. alternata* (Alt) on days 0, 3, 6, and 13. Flow cytometric analysis of cells isolated from the lung of papain- or PBS-challenged animals at day 14 is shown. Panels represent live CD45$^+$ cells stained with Thy1.2 and lineage (Lin) markers (middle). ILCs gated on Lin$^-$ and Thy1.2$^+$ expression (ILC) were stained for GATA3 (ILC2) and Ki67, and total numbers of ILC2s in the lung were quantified (right).

(B) Representative histograms and mean fluorescence intensity (MFI) values of 2-NBDG in lung ILC2 (Lin$^-$ Thy1.2$^+$ ST2$^+$).

(legend continued on next page)

facilitate the maintenance and protection of barrier sites with a fluctuating supply of nutrients, metabolic programs operating in settings of lower glucose may control ILC2 function. Such independence from a high glucose supply may be even more important, since its availability in tissues can be sparse, in contrast to the amounts found in the blood. Indeed, our recent data suggest that tissue-resident ILC2s acquire high amounts of fatty acids (FAs) from the environment and mostly depend on FA metabolism during helminth infection and malnutrition (Wilhelm et al., 2016). Thus, protective ILC2 responses tailored to maintain and repair the epithelial barrier are largely dependent on FA oxidation (FAO). This idea is further supported by the identification of genes involved in FA metabolism as a defining feature of ILC2s (Robinette et al., 2015). Alternatively, expression of the enzyme arginase 1 and arginine catabolism in ILC2s was identified as supporting aerobic glycolysis and pathogenic ILC2 responses in airway inflammation (Monticelli et al., 2016). These data highlight the importance of glycolysis for the development of pathogenic ILC2 responses but also suggest that additional metabolic pathways are likely activated when glucose availability is limited.

Here, we found that pathogenic ILC2s, elicited in the context of allergen-induced airway inflammation, displayed a distinct metabolic phenotype, simultaneously increasing both glucose and FA uptake from the environment. Lipid droplets (LDs) function as transient cellular nutrient buffers to prevent lipotoxicity of externally acquired FAs. Lipid uptake and storage are coupled to glucose availability, and both functions were required to drive proliferation and fuel pathogenic ILC2 responses. Lipid metabolism of ILC2s was found to be controlled by the genes *Dgat1* and *Pparg*. Finally, feeding animals a ketogenic diet resulted in dietary restriction of glucose, impaired lipid metabolism, and ablated ILC2-driven airway inflammation. Thus, our findings identify lipid metabolism as an important metabolic program for ILC2 function and highlight the therapeutic potential of a ketogenic diet to treat airway inflammation.

RESULTS

Chronic Activation Induces LD Formation in Pulmonary ILC2s

Hallmarks of T cell activation are increased glucose uptake and a metabolic switch to aerobic glycolysis to match the high-energy demand required for proliferation, growth, and cytokine production (Pearce et al., 2013). To better understand the metabolic requirements underlying chronic activation of tissue-resident ILC2s, we challenged mice with a protease allergen, papain, which causes ILC2-induced airway inflammation in mice and humans (Halim et al., 2012; Novey et al., 1979; Oboki et al., 2010; Wilhelm et al., 2011). Upon papain exposure, pulmonary ILC2s increased in number, proliferated, and acquired more glucose from the environment, as determined by the uptake of the fluorescent glucose analog 2-NBDG, than ILC2s isolated from PBS-challenged control mice (Figures 1A and 1B). Increased glucose uptake is indicative of a switch to glycolysis and in line with recent data suggesting an important role for glycolysis in the maintenance of pathogenic ILC2s (Monticelli et al., 2016). However, we observed that chronic activation of ILC2s also drastically increased the uptake of external FAs by probing the delivery of the fluorescently labeled long-chain FA palmitate 4,4-Difluoro-5,7-Dimethyl-4-Bora-3a,4a-Diaza-s-Indacene-3-Hexadecanoic Acid (BODIPY FL C_{16}) (Figure 1C). This finding was confirmed by using alkyne-labeled palmitic acid (alkyne-palmitate), which can be detected upon click reaction with an azide-coupled fluorescent reporter (Gaebler et al., 2016) (Figure 1D). We also noted that while the availability of glucose in the lung tissue was reduced in comparison to the amounts measured in the plasma at steady state, glucose concentrations increased in the airways upon exposure to papain (Figure S1A). A similar effect was observed for free FAs (FFAs) (Figure S1B). To test whether increased uptake of glucose and FAs is a general feature of chronically activated ILC2s, we extended our analysis to a model of fungal allergens. Similar to mice challenged with papain, ILC2s accumulated in mice treated with the fungal allergen extract of *Alternaria alternata* and displayed increased uptake of exogenous FAs and glucose (Figures 1E–1G). However, while genes involved in the control of glycolysis, such as *Hk1*, *Ldha*, and *Pkm*, were upregulated, key genes involved in FA oxidation (FAO) (*Ppara*, *Cpt1*, and *Acox1*), FA synthesis (*Acc1*, *Fasn*, and *Acly*), and cholesterol synthesis (*Hmgcs1* and *Srebf1)* were not elevated in ILC2s elicited in the context of papain (Figures 1H and S2A). Instead, we observed a significant upregulation of genes involved in FA uptake (*Pparg* and *Slc27a6*) and genes catalyzing the conversion of diacylglycerol and fatty acyl coenzyme A (CoA) to triglycerides (TGs) (*Dgat1* and *Dgat2*) (Figures 1H and S2B). In particular, the enzyme DGAT1 serves the essential metabolic role of preventing lipotoxicity by funneling potentially toxic FFAs into LDs (Chitraju et al., 2017; Nguyen et al., 2017). Hence, expression of DGAT1 may allow ILC2s to acquire and store exogenous lipids from the tissue microenvironments. To this end, we stained ILC2s with the neutral lipid dye 4,4-difluoro-1,3,5,7,8-pentamethyl-4-bora-3a,4a-diaza-s-indacene (BODIPY 493/503) to quantify neutral lipids, such as TGs, by flow cytometry. Papain- or fungal-allergen-elicited lung

(C and D) MFI values of BODIPY FL C_{16} uptake (C) and MFI values of alkyne-palmitate uptake by lung ILC2s (Lin^- $Thy1.2^+$ $Gata3^+$) after papain or PBS challenge (D).

(E) Total numbers of ILC2s in the lungs of *A.-alternata*-challenged animals.

(F) Representative histograms and MFI values of 2-NBDG in lung ILC2s (Lin^- $Thy1.2^+$ $ST2^+$).

(G) MFI values of BODIPY FL C_{16} uptake after *A. alternata* or PBS challenge.

(H) RT-PCR analysis relative to *Hprt* displayed as fold-change expression of ILC2 from papain- (Pap) over PBS-challenged (Ctrl) mice.

(I–K) Representative histograms and MFI values of BODIPY 493/503 (Lin^- $Thy1.2^+$ $Gata3^+$) from papain- (I) or *A.-alternate*- and PBS-challenged mice (J), and representative microscopic images of BODIPY 493/503 staining in lung ILC2s (Lin^- $Thy1.2^+$ $Gata3^+$) after papain or PBS challenge (K). Scale bar represents 10 μm.

Results show two pooled experiments (A, E, and H) or one representative experiment (B–D, F, G, I, and J) from at least two (D–G, J, and K) or three (A–C and H–I) independent experiments with three to five mice in each experimental group. All graphs display means ± SEM; $^*p \leq 0.05$, $^{**}p \leq 0.01$, and $^{***}p \leq 0.001$. See also Figures S1 and S2.

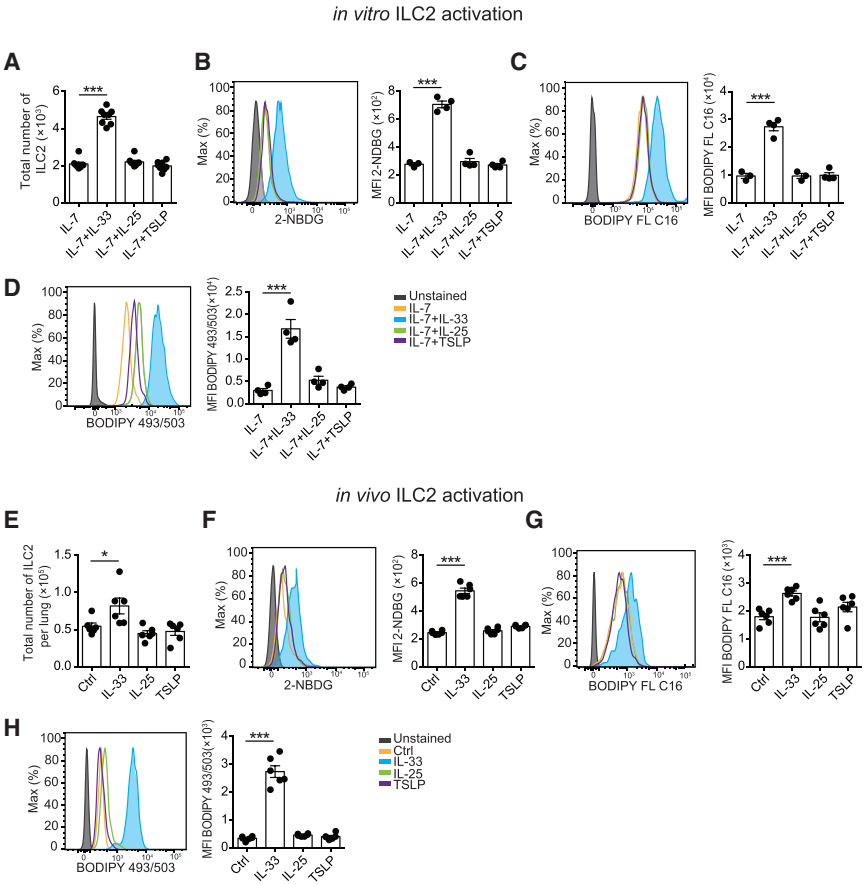

Figure 2. IL-33 Promotes Lipid Uptake and LD Formation in Activated ILC2s

ILC2s were sort purified from naive C57BL/6 mice and cultured for 3 days in the presence of IL-7 or a combination of IL-7 and IL-33, IL-7 and IL-25, or IL-7 and TSLP.

(A) Total numbers of purified ILC2s after 3 days of culture.

(B and C) Representative histograms and MFI values of 2-NBDG (B) and BODIPY FL C_{16} (C) uptake by cultured ILC2s.

(D) Representative histograms and MFI values of BODIPY 493/503 staining in cultured ILC2s.

(E) C57BL/6 mice were challenged intranasally with IL-33, IL-25, TSLP, or PBS on 3 consecutive days. On day 4, cells isolated from the lung of cytokine- and PBS-challenged animals were analyzed by flow cytometry.

(F–H) Representative histograms and MFI values of 2-NBDG in lung ILC2s (F) and BODIPY FL C_{16} uptake (G) and BODIPY 493/503 staining (H) of lung ILC2s (Lin^- $Thy1.2^+$ $Gata3^+$).

Results display two pooled experiments (A, E–H) or one representative experiment of at least three (B–D) independent experiments with three to five mice in each experimental group. All graphs display means ± SEM; $^*p \leq 0.05$, $^{**}p \leq 0.01$, and $^{***}p \leq 0.001$. See also Figure S3.

ILC2s displayed markedly increased staining with BODIPY 493/503, indicative of increased LD formation, when compared to ILC2s isolated from control animals (Figures 1I and 1J). Increased LD formation in activated ILC2s was also confirmed by confocal microscopy (Figure 1K). Thus, ILC2s activated in the context of allergen-driven airway inflammation display a metabolic phenotype characterized by increased uptake of exogenous glucose and FAs, increased glycolysis, and storage of FAs in LDs.

IL-33 Promotes Acquisition of External Lipids and LD Formation in Activated ILC2s

Activation of ILC2s is largely dependent on their exposure to epithelial-derived cytokines such as thymic stromal lymphopoietin (TSLP), IL-25, and IL-33 (Vivier et al., 2018). To address which epithelial factors control the simultaneous increase in glycolysis and FA metabolism in ILC2s, we cultured sort-purified ILC2s (Figure S2C) in the presence of IL-7 alone or in combination with IL-33, IL-25, or TSLP to mimic a steady state or activation of ILC2s, respectively. Notably, only simultaneous exposure of ILC2s to IL-7 and IL-33, but not IL-7 alone (steady state), or in combination with TSLP or IL-25, induced the proliferation of ILC2s and increased the uptake of glucose and external FAs and the formation of LDs (Figures 2A–2D). To further assess the importance of IL-33 in activating a metabolic program that drives pathogenic ILC2 responses *in vivo*, we treated mice intranasally with the cytokines IL-25, IL-33, or TSLP. In line with our *in vitro* experiments, ILC2s accumulated in the airways of mice challenged with IL-33, but not IL-25 or TSLP, and displayed an increased acquisition of external glucose and FAs, which resulted in increased formation of LDs (Figures 2E–2H). Challenge with IL-33 strongly recapitulated the genetic changes in ILC2s that were induced upon papain challenge and upregulated key genes involved in glycolysis (*Hk1*, *Ldha*, and *Pkm*), FA metabolism (*Pparg* and *Slc27a6*), and LD droplet formation (*Dgat1*) (Figure S3). Thus, our *in vitro* and *in vivo* experiments suggested that IL-33 may be sufficient to drive the metabolic program that fuels pathogenic ILC2 responses in airway inflammation. To further test this hypothesis, we treated mice with papain that were genetically deficient for the IL-33 receptor (*Il1rl1*$^{-/-}$ mice) (Townsend et al., 2000). In accordance with our previous results, ILC2s isolated from *Il1rl1*$^{-/-}$ animals displayed reduced uptake of glucose and FA and failed to increase the formation of LD when compared to wild-type (WT) mice (Figures 3A–3D). Together, these data suggest that IL-33 imprints a metabolic program in ILC2s characterized by increased uptake of glucose and FAs, upregulation of glycolysis, and the formation of LDs.

DGAT1-Dependent LD Formation Protects ILC2s from Lipotoxicity and Allows for Increased Uptake of External Lipids

Excess FFAs in the cytoplasm of cells can generate damaging bioactive lipids or disrupt the integrity of mitochondrial membranes, a process referred to as lipotoxicity (Unger et al., 2010). The formation of LD is considered an essential step in preventing FFAs from causing such detrimental effects to cells (Bailey et al., 2015; Listenberger et al., 2003). Here, DGAT1, an

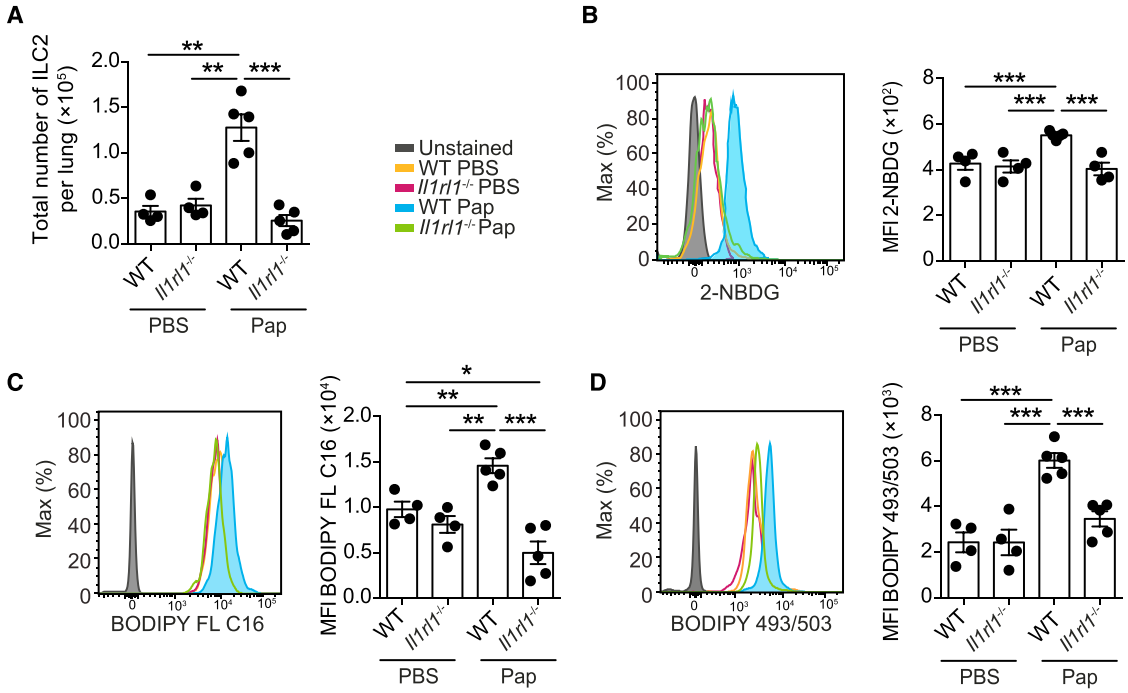

Figure 3. IL-33 Is Essential for Acquisition of External Lipids and LD Formation in ILC2s

(A) WT and *Il1rl1*$^{-/-}$ mice were co-housed and challenged intranasally with papain or PBS (Ctrl) on days 0, 3, 6, and 13, and total numbers of ILC2s were analyzed by flow cytometry and compared to PBS-challenged controls on day 14.

(B–D) Representative histograms and MFI values of 2-NBDG (B), BODIPY FL C_{16} (C), and BODIPY 493/503 (D) in lung ILC2s from C57BL/6 and *Il1rl1*$^{-/-}$ mice challenged with papain or PBS.

Results are representative of at least two independent experiments with three to five mice in each experimental group. All graphs display means ± SEM; *$p \leq 0.05$, **$p \leq 0.01$, and ***$p \leq 0.001$.

enzyme that catalyzes the esterification of diacylglycerides and FAs into TGs, is crucial in the process of LD formation (Garbarino et al., 2009; Nguyen et al., 2017). Esterification and storage in LDs prevents lipotoxicity caused by either excessive uptake of external lipids or the mobilization of FFAs during lipolysis (Chitraju et al., 2017). BODIPY-labeled FAs have been previously used to study lipid trafficking and can be esterified into neutral lipids and stored in LDs (Herms et al., 2013; Kassan et al., 2013; Rambold et al., 2015). To confirm that external lipids scavenged from the environment are indeed stored in LDs, we cultured ILC2s isolated from PBS or papain-challenged mice with 4,4-Difluoro-5,7-Dimethyl-4-Bora-3a,4a-Diaza-s-Indacene-3-Dodecanoic Acid (BODIPY FL C_{12}). Culturing ILC2s with BODIPY FL C_{12} revealed uptake of fluorescently labeled FAs and subsequent storage in LDs, as assessed by confocal microscopy (Figure 4A). To further characterize the subcellular structures that accumulated BODIPY FL C_{12}, we employed imaging flow cytometry. Using this technique, we found that fluorescently labeled lipids strongly co-localized with the protein perilipin-2 (PLIN2), a putative marker for LDs (Figure 4B). In agreement with our confocal microscopy images, the number of LDs and the intensity of BODIPY FL C_{12} signal per cell increased in ILC2s after papain challenge (Figures 4B–4D). To test if expression of DGAT1 allows for the acquisition of external lipids by preventing lipotoxicity in activated ILC2s, we treated purified ILC2s isolated from papain-challenged mice with increasing concentrations of a DGAT1 inhibitor (DGAT1i; A922500) (King et al., 2010). Of note, IL-2 alone potently reactivated ILC2s isolated from papain-challenged mice (Figure S4A) (Wilhelm et al., 2011). In agreement with the essential role of DGAT1 in the formation of LDs, even nontoxic concentrations of DGAT1i reduced the capacity of ILC2s to form LDs (Figure 4E), while 40 μM DGAT1i in culture caused lipotoxicity, as measured by a shift in the emission peak of the fluorescent lipid peroxidation sensor BODIPY 581/591 C_{11} (Figure 4F). Increased lipotoxicity resulted in apoptosis and decreased survival, accumulation, and proliferation of ILC2s reactivated with IL-2 in culture (Figures 4G, 4H, S4B, and S4C). In addition, inhibiting the function of DGAT1 greatly ablated the ability of cells to store external lipids in LDs, as assessed by imaging flow cytometry (Figure 4I). In contrast, blocking the activity of DGAT2, another isoform of diacylglycerol O-acyltransferase expressed in ILC2s (Robinette et al., 2015; Futatsugi et al., 2015), had no effect on ILC2 viability, proliferation, or LD formation in culture (Figures S4D and S4E). This suggests that DGAT1, but not DGAT2, may be essential for ILC2s to acquire and store high amounts of external lipids from the environment. Since high concentrations of extracellular lipids may cause toxicity (Unger et al., 2010), the upregulation of DGAT1 in the context of airway inflammation may render ILC2s less sensitive to the presence of excess amounts of external lipids. Indeed, DGAT1 function was important for the ability of ILC2s to utilize increased amounts of external lipids, and treatment with a nontoxic concentration of DGAT1i impaired their capacity to utilize oleic and linoleic acid or palmitic acid and

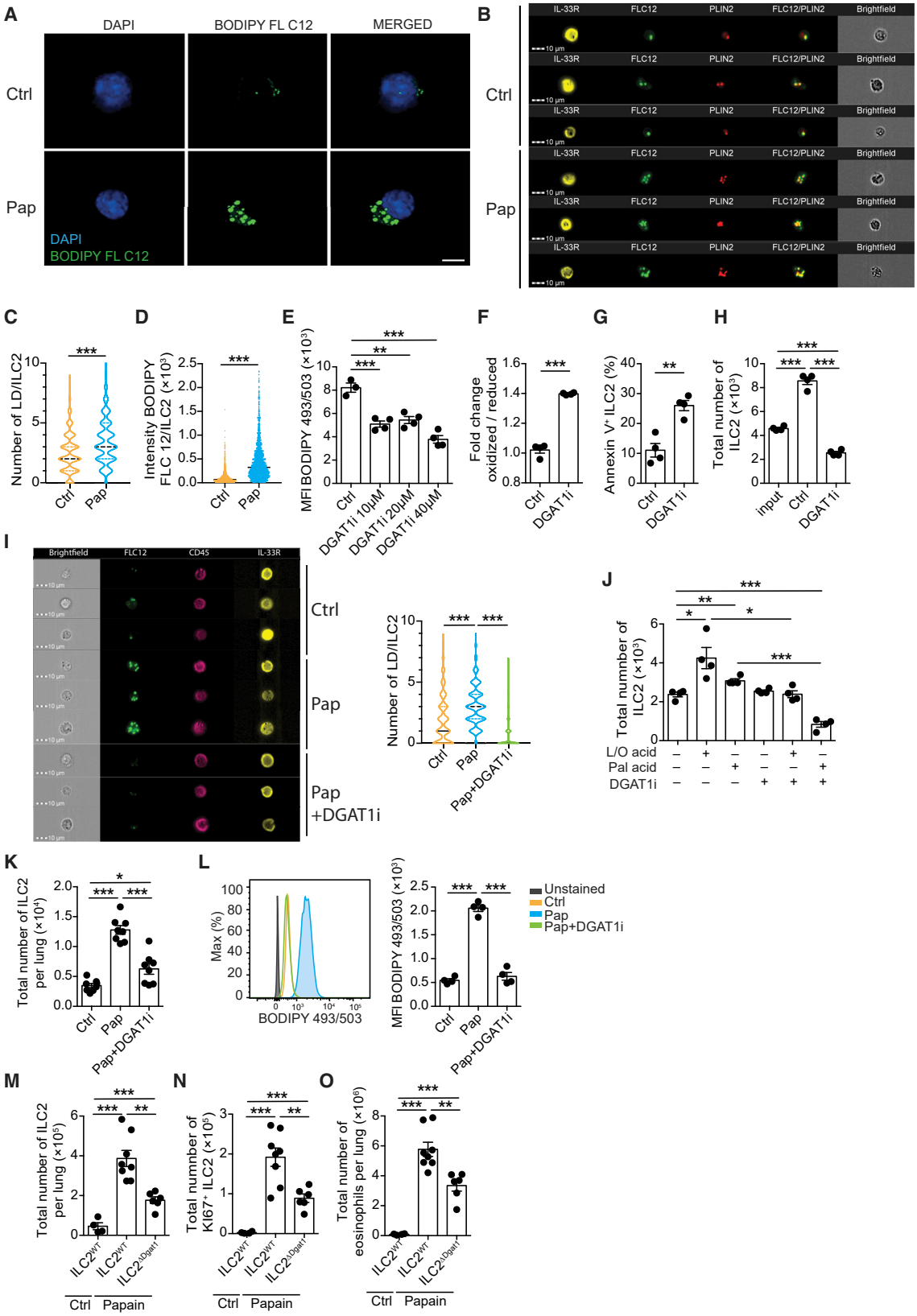

(legend on next page)

proliferate in culture (Figure 4J). Our *in vitro* results suggest that the function of DGAT1 may be essential for chronically activated ILC2s to utilize external lipids. To test the importance of LD formation for the functionality of ILC2s in an inflamed-tissue microenvironment, we treated papain-challenged mice with DGAT1i *in vivo*. Of note, inhibition of DGAT1 almost completely ablated the accumulation of ILC2 in the lungs of papain-challenged mice (Figure 4K). Furthermore, while ILC2 isolated from papain-challenged mice treated with DGAT1i showed no reduction in their capacity to acquire glucose and FAs from the environment, such ILC2s failed to form more LDs (Figures 4L, S4F, and S4G). Finally, to assess the specific function of DGAT1 in ILC2s, we generated mice carrying a specific deletion of DGAT1 in ILC2s by crossing mice expressing the *RFP* gene followed by an internal ribosomal entry site (IRES) and the *CRE* recombinase under the endogenous control of the IL-5 locus (*Red5* mice; Nussbaum et al., 2013) to mice carrying the *loxP*-flanked *Dgat1* gene (*Dgat1*$^{l/fl}$ mice). Since IL-5 is primarily produced by ILC2s in the steady state but also in the context of papain-induced airway inflammation (Nussbaum et al., 2013) (Figure S4H), such mice will specifically delete the *Dgat1* gene in ILC2s (ILC2$^{\Delta Dgat1}$ mice). Analysis of these animals revealed that ILC2s from ILC2$^{\Delta Dgat1}$ mice showed significantly impaired capacity to proliferate and accumulate in allergen-challenged lungs in comparison to their littermate controls (Figures 4M and 4N). Diminished accumulation of ILC2s also reduced other signs of ILC2-mediated allergic inflammation, such as the recruitment of eosinophils to the airways (Figure 4O). In the remaining ILC2s of ILC2$^{\Delta Dgat1}$ mice, we did not detect any difference in the expression of *Dgat1* or their capacity to store neutral lipids in comparison to ILC2^{WT} mice (Figures S4I and S4J). In support of our findings using inhibition of DGAT1, this suggests that a lack of DGAT1 causes lipotoxicity, which results in a rapid disappearance of DGAT1-deficient ILC2s from the airways. Consequently, the remaining ILC2s in ILC2$^{\Delta Dgat1}$ mice may have escaped excision of *Dgat1.* Hence, we hypothesized that reactivation of ILC2s in culture would result in *de novo* deletion of *Dgat1* in the remaining cells. In agreement with the importance of DGAT1 for the formation of LDs and ILC2 function, ILC2s purified from papain-challenged ILC2$^{\Delta Dgat1}$ mice and reactivated in culture displayed decreased *Dgat1* expression, LDs, proliferation, and accumulation in culture in comparison to ILC2s isolated from ILC2^{WT} mice (Figures S4K–S4N). We confirmed this finding by using a cell-permeable Cre recombinase (Tat-Cre) to acutely delete *Dgat1* from cultured ILC2s isolated from *DGAT1*$^{fl/fl}$ animals (Figures S4O–S4R). Thus, DGAT1 expression in ILC2s mediates the formation of LDs, which act as an essential nutrient-buffering system in activated ILC2s to allow the acquisition of high amounts of external FAs while avoiding lipotoxicity.

PPARγ-Regulated Uptake of Exogenous FAs Fuels Proliferation and Cytokine Production

Since glucose availability is lower in tissues than in blood (Figure S1A), FAs may be an important additional fuel source for tissue-resident ILC2s in chronic airway inflammation. To directly test the effects of external FAs on ILC2s, we added the long-chain FAs linoleic acid, oleic acid, and palmitic acid to cultured ILC2s. In line with our previous results (Figure 4J), addition of external FAs substantially increased both the proliferation and accumulation of ILC2s in culture (Figures 5A–5D). In addition, highly proliferative cells (assessed by intracellular Ki67 staining) stored and acquired more external lipids in LDs than non-cycling cells (Figures S5A and S5B). Increased lipid acquisition in highly proliferative cells was confirmed by assessing the uptake of alkyne-palmitate in ILC2s isolated from papain-challenged mice (Figure S5C). Gene expression analysis of ILC2s that were activated upon papain challenge did not reveal any substantial upregulation of genes involved in *de novo* lipid synthesis (Figure 1E). Thus, we hypothesized that externally acquired FAs may be used directly to build membranes to support proliferation. To test this idea, we performed a pulse-chase experiment with the addition of alkyne-Palmitate to cultured ILC2s. After one night of culture with alkyne-palmitate (0 h), we found accumulation in LDs, as visualized by confocal microscopy (Figure 5E, upper panel). However, after an additional 24 h of culture without alkyne-palmitate, the signal in LD had weakened and the remaining alkyne-palmitate localized to the cellular membrane, indicative of a potential conversion of exogenously acquired palmitic acid into membranous

Figure 4. DGAT1-Dependent LD Formation Protects ILC2s from Lipotoxicity and Allows for Increased Uptake of External Lipids

(A) Representative microscopic images of purified ILC2s isolated from papain- (Pap) or PBS-challenged (Ctrl) mice cultured in the presence of IL-2 and BODIPY FL C_{12}. Scale bar represents 10 μm.

(B–D) Imaging flow cytometry of purified ILC2s (B), violin plots depicting the total number of LDs per ILC2 identified by co-staining for PLIN2 and BODIPY FL C_{12} (C), and fluorescence intensity of BODIPY FL C_{12} per ILC2 (D).

(E) MFI values of BODIPY 493/503 staining in ILC2s purified from papain-challenged C57BL/6 mice and cultured for 3 days with increasing concentrations of the DGAT1 inhibitor A922500 (DGAT1i).

(F) Ratios of the fluorescent emission peaks of the lipid peroxidation sensor BODIPY 581/591 C_{11} at 510/590 nm in ILC2s purified from papain-challenged C57BL/6 mice and cultured for 3 days in the presence of IL-2 with 20 μM DGAT1i.

(G and H) Annexin V staining (G) and total numbers of ILC2s (H) after 3 days of culture in comparison to the number of cultured cells at day 0 (input).

(I) Imaging flow cytometry of ILC2s purified from papain-challenged animals and cultured in the presence of IL-2 and BODIPY FL C_{12} with or without DGAT1i (20 μM) (left panel), and violin plots depicting the total number of LDs per ILC2 (right panel).

(J) Culture of ILC2s with linoleic acid-BSA and oleic acid-BSA (l/o) or palmitic acid-BSA (pal) and a nontoxic concentration of DGAT1i (20 μM).

C57BL/6 mice were challenged intranasally with papain or PBS on days 0, 3, 6, and 13 and simultaneously treated intraperitoneally (i.p.) with DGAT1i, and control animals were treated with DMSO only.

(K) Total numbers of ILC2s from PBS- (Ctrl), papain- (Pap), or papain-challenged mice treated with DGAT1i (Pap+DGAT1i).

(L) Representative histograms and MFI values of BODIPY 493/503 in ILC2 (Lin$^-$ Thy1.2$^+$ Gata3$^+$).

(M–O) Flow cytometric analysis of total numbers of ILC2s (M), Ki67$^+$ ILC2s (N), or eosinophils (O) from control (Ctrl) or papain-challenged (Papain) ILC2^{WT} and ILC2$^{\Delta Dgat1}$ mice.

Results are representative of at least two (A–E, J, and L) or three (F–H) independent experiments or display two pooled experiments (K and M–O) with three to five mice in each experimental group or 2,000 cells of one experiment (I). All graphs display means ± SEM; *$p \leq 0.05$, **$p \leq 0.01$, and ***$p \leq 0.001$. See also Figure S4.

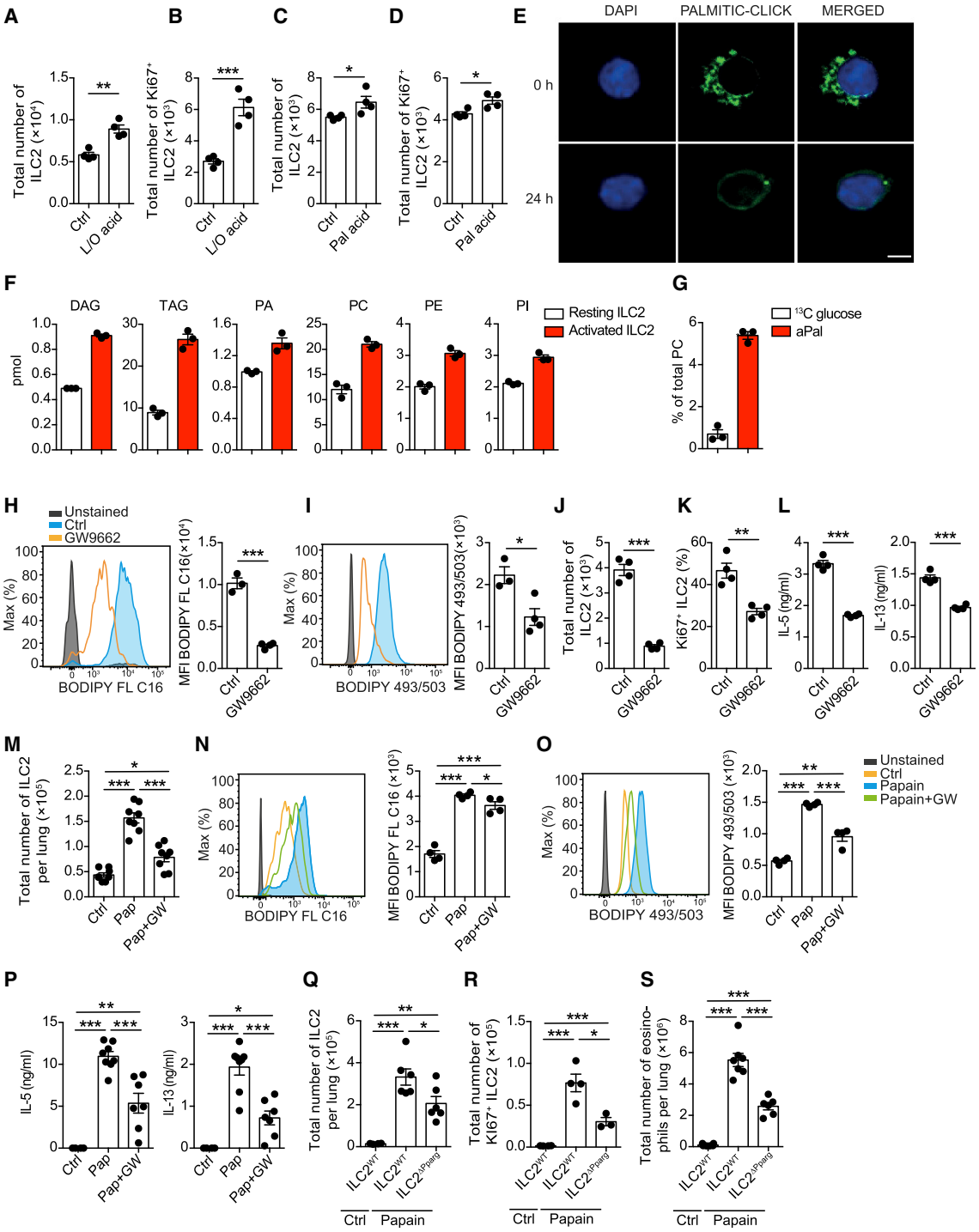

Figure 5. PPARγ-Regulated Uptake of Exogenous FAs Fuels Proliferation and Cytokine Production

(A–D) Total numbers of (A) purified lung ILC2s and (B) Ki67$^+$ ILC2s isolated from papain-challenged C57BL/6 mice cultured for 3 days with IL-2 in the presence or absence of linoleic acid-BSA and oleic acid-BSA (l/o), and total numbers of ILC2s(C) and Ki67$^+$ ILC2s (D) cultured with palmitic acid-BSA (pal).

(E) Representative microscopic images of purified ILC2 isolated from papain-challenged mice pulsed with alkyne-palmitate-BSA overnight and chased for 0 or 24 h. Scale bar represents 10 μm.

(F) Total amounts of alkyne-labeled lipids in ILC2s isolated on day 14 from mice challenged with papain on days 0, 3, 6, and 13 (activated ILC2s) or days 0, 3, and 6 (resting ILC2s).

(G) Relative abundance of labeled ^{13}C-glucose and alkyne-palmitate (aPal) in phosphatidylcholine (PC)

Purified ILC2s were cultured in the presence or absence of the PPARγ inhibitor GW9662.

(legend continued on next page)

phospholipids (Figure 5E, lower panel). To further assess the fate of externally acquired FAs on the molecular level, we employed lipid tracing using alkyne-palmitate coupled to lipidomic analysis (Thiele et al., 2019). In agreement with our hypothesis, we found that externally acquired lipids were not only incorporated in TGs found in LDs but also further metabolized into phospholipids, such as phosphatidylcholine (PC) (Figure 5F). This process was markedly enhanced in ILC2s isolated from mice acutely exposed to allergens in comparison to ILC2s isolated from animals exposed to papain 7 days before analysis without re-challenge (Figure 5F). In contrast, the percentage of phospholipids directly synthesized from glucose was much lower in acutely activated ILC2s, which we analyzed by tracing the incorporation of ^{13}C glucose into PC (Figure 5G). To further test if external lipids may be used to fuel the increased energy demand of activated ILC2s, we used a Seahorse extracellular flux analyzer to compare the bioenergetic profiles of ILC2s. Addition of extracellular lipids had no significant effects on the basal mitochondrial respiration but elevated the spare respiratory capacity (SRC) (Figure S5D). In contrast, the addition of glucose increased basal respiration of ILC2s (Figure S5E). Taken together these results suggest that externally acquired lipids may be predominately used for generation of the phospholipids required for proliferation of activated ILC2s, whereas glucose could be used to fuel the increased energy demand of activated ILC2s. To further understand the control of FA metabolism in ILC2s, we turned to the investigation of potential transcriptional regulators. PPARγ is an essential regulator of FA metabolism, including FA uptake and LD formation, in adipose tissue and liver (Ahmadian et al., 2013), and papain challenge led to an upregulation of PPARγ in ILC2s (Figure 1E). To test the function of PPARγ as an essential factor driving lipid metabolism in papain-elicited ILC2s, we cultured ILC2s in the presence or absence of GW9662, a specific PPARγ inhibitor (Bendixen et al., 2001; Huang et al., 1999). We found that ablation of PPARγ function in purified ILC2s reduced the uptake of external FAs and the formation of LDs by reducing the expression of *Dgat1* (Figures 5H, 5I, and S5F). As a consequence, the capacity of ILC2s to proliferate and expand in culture was impaired, as was the production of effector cytokines from ILC2 in culture (Figures 5J–5L). Hence, PPARγ appears to fuel proliferation and cytokine production of ILC2s by directly regulating the uptake and storage of external FAs in LDs. To test the importance of PPARγ for the function of ILC2s in the inflamed tissue microenvironment, we treated papain-challenged mice with GW9662. Inhibition of PPARγ drastically reduced the numbers of papain-induced ILC2s in the airways and decreased the capacity of ILC2s to take up and store FAs in LDs, while their capacity to acquire glucose from the environment was unchanged (Figures 5M–5O and S5G). PPARγ inhibition also drastically reduced the production of the ILC2 effector cytokines IL-5 and IL-13 in the lung tissue (Figure 5P). To assess the specific function of PPARγ in ILC2s, we crossed *Red5* mice to *Pparγ*$^{fl/fl}$ animals to generate mice with a specific deletion of PPARγ in ILC2s (ILC2$^{\Delta Pparg}$ mice). ILC2$^{\Delta Pparg}$ mice challenged with papain showed reduced numbers of ILC2s and eosinophils in the airways, in contrast to their littermate controls, thus confirming the ILC2-intrinsic importance of PPARγ for fueling pathogenic ILC2s (Figures 5Q–5S). In line with the effects observed in ILC2$^{\Delta Dgat1}$ mice, we were unable to detect lower PPARγ expression or reduced uptake and storage of FAs in LDs in the remaining ILC2s isolated from ILC2$^{\Delta Pparg}$ mice (Figures S5H–S5J). Thus, the remaining ILC2s have probably escaped excision of the *Pparg* gene. This hints at a substantially reduced survival and functionality of *Pparγ*$^{-/-}$ ILC2s *in vivo* and further emphasizes the importance of PPARγ-driven lipid metabolism in ILC2s. However, reactivation of ILC2s isolated from papain-challenged ILC2$^{\Delta Pparg}$ mice in culture resulted in decreased expression of PPARγ, proliferation, and accumulation and reduced their capacity to take up and store FAs in LDs in comparison to ILC2s isolated from ILC2^{WT} mice (Figures S5K–S5O). Thus, the acquisition of external FAs by ILC2s appears to fuel the proliferation process and is controlled by PPARγ, which regulates the coordinated uptake of external lipids and the subsequent storage in LDs to prevent lipotoxicity. As a correlative, inhibition or genetic deletion of PPARγ largely impairs the metabolic pathways fueling the accumulation and effector functions of ILC2s in the inflamed airways.

Glucose and External FAs Cooperate to Fuel FA Metabolism in ILC2s

Since we observed increases in both glucose and FA metabolism in activated ILC2s, we speculated that the presence of glucose may play an essential role in the ability of ILC2s to acquire FAs from the environment. To test this supposition, we assessed the ability of ILC2s to obtain FFAs from the environment and their capacity to store acquired lipids in LDs in the absence of glucose. ILC2s cultured in the absence of glucose decreased their uptake of external lipids and the formation of LDs (Figures 6A and 6B). The reduced capacity to acquire external lipids diminished the overall number of ILC2s in culture, lowered cytokine production, and resulted in a marked downregulation of *Dgat1* and *Pparg* (Figures 6C–6E). This implies that glucose availability may regulate the expression of *Pparg* and thus the capacity to acquire external lipids and form LDs. To further understand the molecular control of this mechanism, we investigated the role of nutrient sensors in the regulation of ILC2 lipid metabolism. mTOR is an essential nutrient sensor, integrating signaling

(H–L) Representative histograms and MFI values of BODIPY FL C_{16} uptake (H), MFI values of BODIPY 493/503 in cultured ILC2s (I), and total numbers of ILC2s (J), Ki67-expressing ILC2s (K), and cytokines (L) in the supernatant after 3 days of culture.

C57BL/6 mice were challenged intranasally with papain or PBS on days 0, 3, 6, and 13 and simultaneously treated i.p. with GW9662. Control animals were treated with DMSO only.

(M) Total numbers of ILC2s from PBS- (Ctrl), papain-challenged (Pap) mice treated with GW9662 (Pap+GW) on day 14.

(N and O) Representative histograms and MFI values of BODIPY FL C_{16} uptake (N) and BODIPY 493/503 (O) in ILC2s (Lin$^-$ Thy1.2$^+$ Gata3$^+$).

(P) Cytokine concentration of IL-5 and IL-13 in the lung homogenate.

(Q–S) Flow cytometric analysis of total numbers of ILC2s (Q), Ki67$^+$ ILC2s (R), or eosinophils(S) from control (Ctrl) or papain-challenged (Papain) ILC2^{WT} and ILC2$^{\Delta Pparg}$ mice.

Results are representative of at least one (G), two (A–F), or three (H–L, N, and O) independent experiments or display two pooled experiments (M and P–S) with three to five mice in each experimental group. All graphs display means ± SEM; *$p \leq 0.05$, **$p \leq 0.01$, and ***$p \leq 0.001$. See also Figure S5.

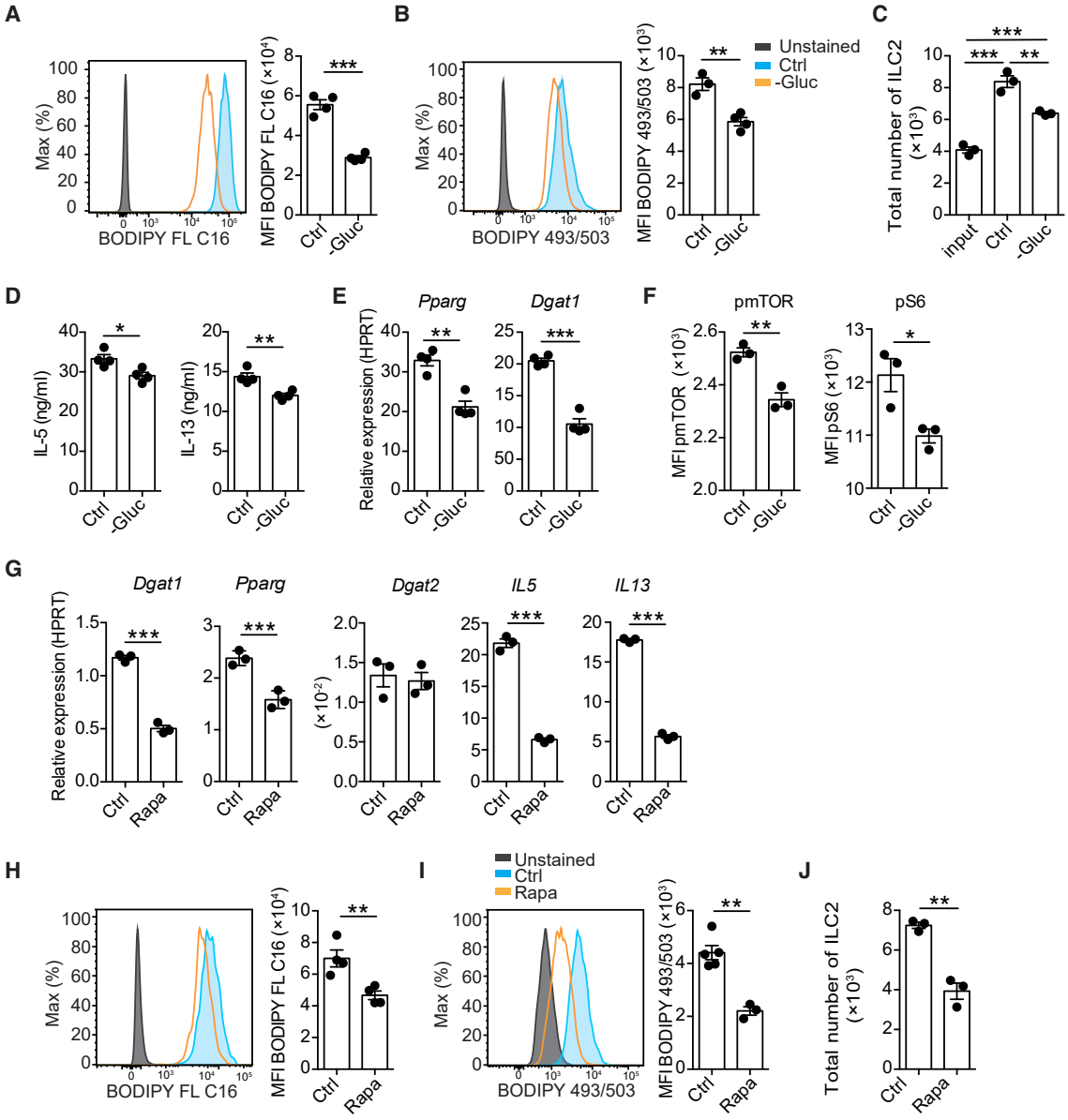

Figure 6. Glucose and External FAs Cooperate to Fuel FA Metabolism in ILC2s

(A and B) Representative histograms and MFI values of BODIPY FL C_{16} uptake (A) and MFI values of BODIPY 493/503 staining (B) in cultured ILC2s.

(C and D) Total numbers of purified lung ILC2 from papain-challenged C57BL/6 mice cultured for 3 days with IL-2 in the presence (+Gluc) or absence of glucose (−Gluc) in comparison to the number of cultured cells at day 0 (input) (C) and cytokines in the supernatant of these cells after 3 days of culture (D).

(E and F) RT-PCR analysis relative to *Hprt* of ILC2s cultured in the presence or absence of glucose (E) and MFI values of intracellular phospho-mTOR and phopho-S6 (F).

(G) RT-PCR analysis relative to *Hprt* of ILC2 cultured for 3 days in the presence (Rapa) or absence (Ctrl) of 5 nM rapamycin.

(H–J) Representative histograms and MFI values of BODIPY FL C_{16} uptake (H) and BODIPY 493/503 staining (I), and total numbers of ILC2s in culture (J).

Results are representative of at least two independent experiments with three to four replicates in each experimental group. All graphs display means ± SEM; $^{*}p \leq 0.05$, $^{**}p \leq 0.01$, and $^{***}p \leq 0.001$.

pathways associated with nutrient availability and cellular energy status (Powell and Delgoffe, 2010). Previous data in T cells suggest that mTOR regulates FA metabolism in T cells by controlling PPARγ (Angela et al., 2016). While glucose deprivation reduced both mTOR S2448 phosphorylation and phosphorylation of the mTOR target S6, addition of the mTOR inhibitor rapamycin reduced expression of both *Dgat1* and *Pparg* (Figures 6F and 6G). In line with our previous findings, rapamycin-mediated suppression of *Dgat1* and *Pparg* resulted in decreased expression of cytokines and reduced the capacity of ILC2s to acquire external lipids and storage in LDs (Figures 6G–6I). mTOR inhibition not only impaired lipid metabolism but also diminished the ability of ILC2s to proliferate and accumulate in culture (Figure 6J). In summary, our data strongly suggest a mechanism by which the

availability of glucose is coupled to the ability to acquire FAs from the environment to fuel activation of pathogenic ILC2s. This integration of glucose and FA metabolism in ILC2s appears to be mediated by mTOR controlling the expression of *Pparg* and *Dgat1*.

Ketogenic Diet Abrogates ILC2-Driven Airway Inflammation

Altogether, our findings suggest that the pathogenic function of ILC2s may be controlled by a simultaneous increase in the capacity of ILC2s to utilize glucose and FAs. Hence, we hypothesized that actively influencing the metabolic status of the host by restraining the availability of dietary glucose may ablate the capacity of ILC2s to increase acquisition of external FAs to fuel airway inflammation. A reduction in glucose availability can be achieved by feeding mice a ketogenic diet, which has a fat to protein and carbohydrate ratio of ~4:1 (Kennedy et al., 2007; Lutas and Yellen, 2013). Indeed, feeding animals a ketogenic diet increased the amounts of ketone bodies found in circulation (Figure S6A). Animals fed a ketogenic diet displayed drastically reduced airway infiltration with eosinophils and ILC2s upon papain challenge (Figures 7A and 7B). This effect was restricted to chronically activated ILC2s, since dietary limitation of glucose had no effect on the number of ILC2s or eosinophils recovered from other organs or the lungs in steady state (Figures S6B and S6C). In addition, we observed a pronounced reduction in ILC2-derived cytokines (IL-5 and IL-13) in the lung tissue (Figures 7C and 7D). Histological analysis and staining for mucus-producing cells by periodic acid-Schiff (PAS) assay revealed that papain-challenged mice had increased amounts of cellular infiltrates and mucus-producing cells, both of which are signs of airway pathology (Figure 7E). In contrast, feeding mice a ketogenic diet entirely abrogated mucus production and cellular infiltration in the airways (Figure 7E). While the capacity of ILC2s to acquire glucose was not altered (Figure 7F), the amount of glucose in the lung tissue and circulation was reduced (Figure S6E). In addition, *Pparg* and *Dgat1* expression declined (Figure S6F), which decreased the ability of ILC2s isolated from ketogenic mice to scavenge FAs from the environment to store in LDs (Figures 7F–7H). Coinciding with the diminished availability of glucose, ILC2s from ketogenic mice displayed reduced mTOR signaling (Figures 7I and 7J). This is in line with our findings that glucose deprivation impairs mTOR activation in ILC2s and literature showing that mTOR inhibition with rapamycin impairs ILC2-driven airway inflammation (Salmond et al., 2012). Finally, the suppressive effect of the ketogenic diet appears to be independent of the microbiota, since treatment with antibiotics did not impact the capacity of the ketogenic diet to suppress airway inflammation (Figures S6G–S6L). Thus, ketogenic programs potently restrain a host metabolic program that drives ILC2-mediated airway inflammation by lowering the availability of glucose, impairing mTOR signaling, and consequently impairing FA metabolism in ILC2s.

DISCUSSION

ILCs are an integral component of the tissue barrier, providing immunological and physical protection by repairing the epithelial barrier. However, changes in lifestyle coinciding with industrialization have markedly influenced the incidence of chronic inflammation and ILC-mediated pathologies. In the present study, we found evidence that the pathogenic functions of ILC2s rely on the uptake of extracellular glucose and FAs for proliferation and accumulation in inflamed lung tissue. Our study reveals that glucose alone is not sufficient to allow for expansion of ILC2s in the context of airway inflammation. In general, the availability of glucose in tissues is low compared to the amounts of glucose transported in the blood. Hence, tissue-resident ILC2s may utilize a combination of glucose and FAs to fuel effector functions in the lung tissue. Our findings suggest that increased uptake of exogenous FAs by tissue-resident ILC2s may be particularly important to mediate proliferation by providing lipids for the generation of membrane phospholipids, as shown by lipid tracing experiments. On a cellular basis, it may be more efficient to use exogenous lipids directly to build up membrane components. Hence, this process appears to be preferred over *de novo* phospholipid synthesis from glucose and thus differs from the metabolic program of other cells involved in type 2 immunity (Pelgrom and Everts, 2017). Indeed, recent reports suggest that highly proliferating cells rely on external FAs to build complex lipids for cellular membranes (Yao et al., 2016). In this context, the formation of LDs in ILC2s is an essential process that allows for continuous high uptake of FAs from the environment and prevents lipotoxicity caused by excess intracellular FFAs. Our data suggest that esterification of FFAs into TGs, a process mediated by the enzyme DGAT1, is also critical to fuel pathogenic ILC2s that are elicited in airway inflammation. Pharmacologically or genetically blocking the function of DGAT1 severely impaired the viability of ILC2 in the inflamed lung tissue. Formation of LD is the main system for nutrient buffering, which allows for efficient storage of highly energetic fuels, a process that is mainly active in adipose tissue (Marcelin and Chua, 2010). Here, we have shown that this mechanism is also essential for fueling ILC2s in airway inflammation. Being able to store nutrients in immune cells in general and in ILC2s in particular may serve different functions. On one hand, ILC2s, acting as central effector immune cells responsible for tissue maintenance and repair, are required to operate under fluctuating nutrient availability. Thus, being able to store FAs in LDs may allow ILC2s to function even at times of dietary restriction. On the other hand, glucose concentrations in tissues are low, while FAs may be more abundant. In this context, the process of tissue remodeling after injury not only requires activation of ILC2s but may also provide an ample supply of FAs freed from the membranes of dying cells (Iturralde et al., 2003). A recent report suggests that the mobilization of FFAs from phospholipids by the phospholipase PLA2G5 (expressed on macrophages) is important to support ILC2-driven airway inflammation (Yamaguchi et al., 2018). Thus, a microenvironment of injury and tissue remodeling may provide an abundant supply of FAs, which require temporary storage in LDs to prevent lipotoxicity. ILC2s, as essential mediators of tissue repair and maintenance, have developed mechanisms to evade the toxic effects of environments with high lipid content. Furthermore, our data suggest that lipid uptake and the storage of FFAs in LDs are regulated by PPARγ, since selective inhibition of PPARγ or cell-specific deletion of it directly suppress the acquisition of FAs, LD formation, and proliferation and accumulation of ILC2s in airway inflammation. This finding is in line with previous reports showing the importance of PPARγ

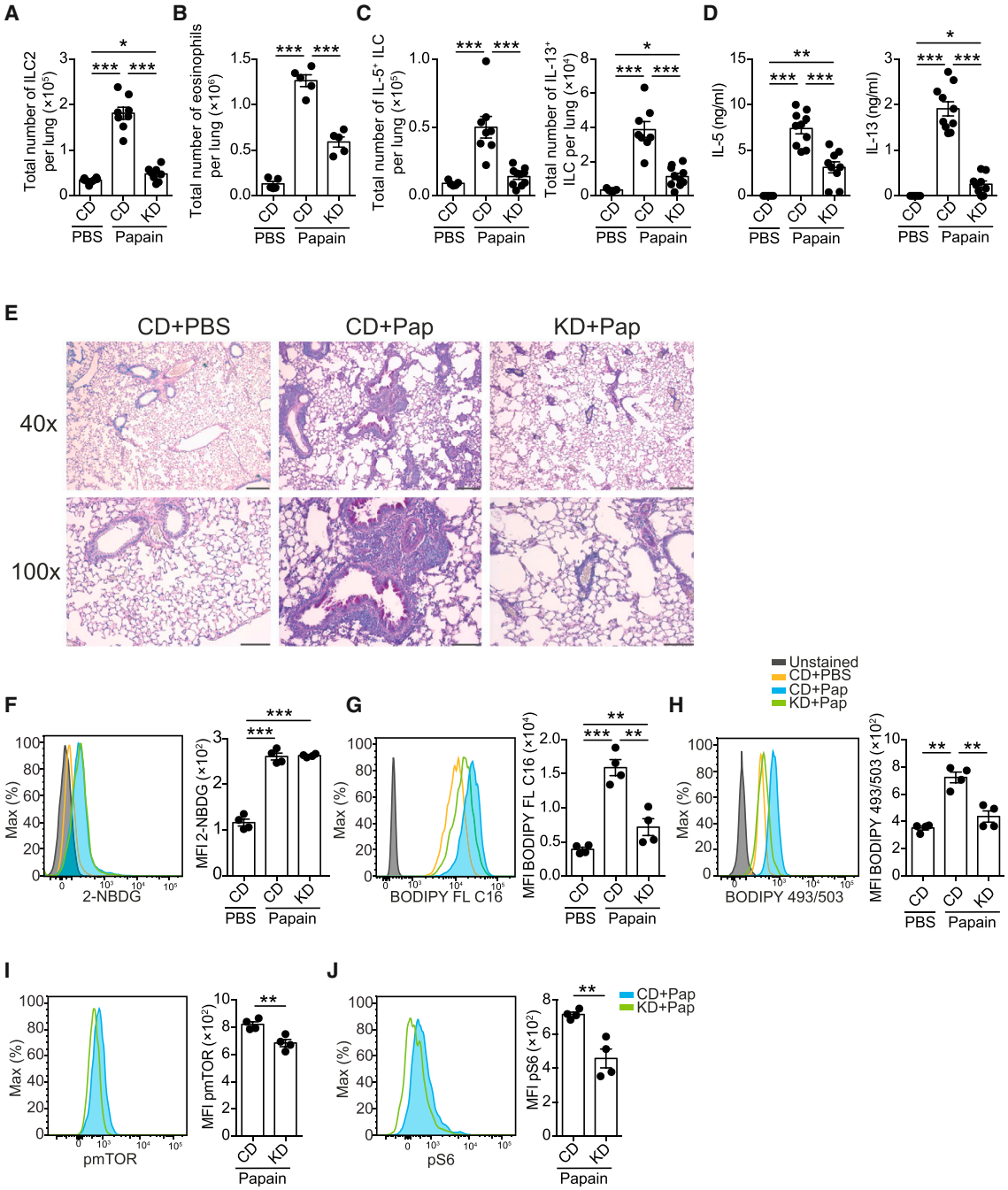

Figure 7. Ketogenic Diet Inhibits ILC2-Driven Airway Inflammation

(A–C) C57BL/6 mice were placed on either a control or ketogenic diet and challenged intranasally with papain or PBS on days 0, 3, 6, and 13. Flow cytometric analysis of total numbers of ILC2s (A), eosinophils (B), and IL-5- and IL-13-producing ILC2s (C) in the lung tissue of PBS-challenged mice fed a control diet (CD) or papain-challenged mice fed a control diet (CD+Pap) or ketogenic diet (KD+Pap).

(D) Cytokine concentration in the lung homogenate.

(E) Histology and PAS staining in the lung tissue. Scale bar represents 200 μm (40×) or 100 μm (100×).

(F–H) Representative histograms and MFI values of 2-NBDG in lung ILC2s (Lin^- $Thy1.2^+$ $ST2^+$) (F), MFI values of BODIPY FL C_{16} uptake (G), and MFI values of BODIPY 493/503 analyzed in lung ILC2s (Lin^- $Thy1.2^+$ $Gata3^+$) (H).

(I and J) Representative histograms and MFI values of intracellular phospho-mTOR (I) and phoshpho-S6 staining (J) in lung ILC2s.

Results display two pooled experiments (A–D) or are representative of at least two (E and I–J) or three (F–H and J) independent experiments with three to five mice in each experimental group. All graphs display means ± SEM; *$p \leq 0.05$, **$p \leq 0.01$, and ***$p \leq 0.001$. See also Figure S6.

for T cell activation by direct regulation of genes controlling the uptake of external lipids (Angela et al., 2016). We found the expression of both *Dgat1* and *Pparg* to be controlled by the availability of glucose, particularly via the nutrient sensor mTOR. This suggests that the availability of glucose controls the proliferation of ILC2s by allowing the uptake and storage of external lipids in LDs. A possible explanation for this cross-regulation is that mitochondria in close contact with LDs require pyruvate from glycolysis to supply ATP, generated via oxidative phosphorylation, for TG synthesis (Benador et al., 2018). Indeed, our data, in line with previous findings (Monticelli et al., 2016), suggest that glucose could be used to drive mitochondrial respiration in papain-activated ILC2s. As a consequence, the increased incidence of chronic airway inflammation in the Western world may be largely mediated by a simultaneous rise in the consumption of carbohydrates and fat. Recent studies have shown an increase in ILC2 responses in the context of high-fat-diet-induced obesity (Everaere et al., 2016). In contrast, our data suggest that the changes induced in host metabolism through a ketogenic diet may be an efficient way to treat airway inflammation. In our model, ketogenesis appeared to block all central aspects of disease development by not only limiting the availability of glucose but also simultaneously reducing the acquisition of exogenous FAs, possibly by reducing mTOR signaling. Ketogenic diets are already used in the clinic to treat epilepsy (Neal et al., 2009) and could also be an efficient way to treat airway inflammation. Such clinical intervention, if proven successful, would be a cost-effective treatment for asthma and allergies. In this regard, it will also be important to consider the genetic and physiological adaptations that have occurred in populations evolved to consume high amounts of fat (Fumagalli et al., 2015). Overall, we have uncovered the acquisition and transient storage of lipids in LDs as an essential mechanism to mediate pathogenic ILC2 responses and a ketogenic diet as a potential treatment for allergen-induced airway inflammation that could be translated into the clinic in the near future.

STAR★METHODS

Detailed methods are provided in the online version of this paper and include the following:

- KEY RESOURCES TABLE
- LEAD CONTACT AND MATERIALS AVAILABILITY
- EXPERIMENTAL MODEL AND SUBJECT DETAILS
  - Animals
- METHOD DETAILS
  - Cell isolation from tissues and flow cytometry
  - Re-stimulation of cells for intracellular cytokine staining
  - Fluorescence-activated cell sorting, purification, and *in vitro* culture of ILC
  - Neutral lipid staining and uptake of 2-NBDG and BODIPY
  - Flow cytometric determination of apoptosis (Annexin V / propidium iodide staining)
  - Lipid peroxidation staining
  - Alkyne-labeled palmitic acid uptake and staining
  - Lipid tracing of alkyne-labeled palmitic acid and lipidomic analysis
  - Lipid tracing of ^{13}C-labeled glucose
  - Metabolic assays
  - *In vitro* TAT-Cre treatment of ILC2
  - Imaging flow cytometry
  - *In vivo* inhibitor treatment
  - Antibiotic treatment
  - Measurement of free fatty acids, glucose, and ketone bodies
  - Histology
  - Confocal microscopy
  - Real-time PCR
- QUANTIFICATION AND STATISTICAL ANALYSIS

SUPPLEMENTAL INFORMATION

Supplemental Information can be found online at https://doi.org/10.1016/j.immuni.2020.03.003.

ACKNOWLEDGMENTS

This work was supported by the Ministry for Science and Education of North-Rhine-Westphalia and the Human Frontiers Science Program (HFSP). C.W., C.T., and M.H. were further supported by the Deutsche Forschungsgemeinschaft (DFG; German Research Foundation) under Germany's Excellence Strategy (EXC2151-390873048 and SPP1937; C.W.). We thank Dr. Richard Locksley providing *Red5* mice and Dr. Andrew McKenzie for *Il1rl1*$^{-/-}$ mice; the animal facility staff for animal care at the UKB (HET); staff from the UKB flow core facility; Andreas Dolf, Peter Wurst, and Maximilian Germer for expert cell sorting; and the UKB Imaging Core Facility. We thank Drs. Meghan Campbell, Bernardo Franklin, and Florian Schmidt; the Wilhelm lab; and Emma Bawden for critical discussions regarding the manuscript.

AUTHOR CONTRIBUTIONS

F.K. and S.K.M. designed and performed the experiments. V.S., A.K., M.M., and J.S. provided experimental help. M.H. provided expertise in data analysis. K.W. and C.T. performed lipid tracing and lipidomic analysis. C.W. designed and performed the experiments and wrote the manuscript.

DECLARATION OF INTERESTS

The authors declare no competing interests.

Received: November 27, 2018
Revised: January 31, 2020
Accepted: March 12, 2020
Published: April 7, 2020; corrected online April 30, 2020

REFERENCES

Ahmadian, M., Suh, J.M., Hah, N., Liddle, C., Atkins, A.R., Downes, M., and Evans, R.M. (2013). PPARγ signaling and metabolism: the good, the bad and the future. Nat. Med. *19*, 557–566.

Anderson, G.P. (2008). Endotyping asthma: new insights into key pathogenic mechanisms in a complex, heterogeneous disease. Lancet *372*, 1107–1119.

Angela, M., Endo, Y., Asou, H.K., Yamamoto, T., Tumes, D.J., Tokuyama, H., Yokote, K., and Nakayama, T. (2016). Fatty acid metabolic reprogramming via mTOR-mediated inductions of PPARγ directs early activation of T cells. Nat. Commun. *7*, 13683.

Artis, D., and Spits, H. (2015). The biology of innate lymphoid cells. Nature *517*, 293–301.

Bach, J.F. (2002). The effect of infections on susceptibility to autoimmune and allergic diseases. N. Engl. J. Med. *347*, 911–920.

Bailey, A.P., Koster, G., Guillermier, C., Hirst, E.M., MacRae, J.I., Lechene, C.P., Postle, A.D., and Gould, A.P. (2015). Antioxidant role for lipid droplets in a stem cell niche of Drosophila. Cell *163*, 340–353.

Benador, I.Y., Veliova, M., Mahdaviani, K., Petcherski, A., Wikstrom, J.D., Assali, E.A., Acin-Perez, R., Shum, M., Oliveira, M.F., Cinti, S., et al. (2018). Mitochondria bound to lipid droplets have unique bioenergetics, composition, and dynamics that support lipid droplet expansion. Cell Metab. *27*, 869–885.e866.

Bendixen, A.C., Shevde, N.K., Dienger, K.M., Willson, T.M., Funk, C.D., and Pike, J.W. (2001). IL-4 inhibits osteoclast formation through a direct action on osteoclast precursors via peroxisome proliferator-activated receptor gamma 1. Proc. Natl. Acad. Sci. USA *98*, 2443–2448.

Buck, M.D., O'Sullivan, D., and Pearce, E.L. (2015). T cell metabolism drives immunity. J. Exp. Med. *212*, 1345–1360.

Chitraju, C., Mejhert, N., Haas, J.T., Diaz-Ramirez, L.G., Grueter, C.A., Imbriglio, J.E., Pinto, S., Koliwad, S.K., Walther, T.C., and Farese, R.V., Jr. (2017). Triglyceride synthesis by DGAT1 protects adipocytes from lipid-induced ER stress during lipolysis. Cell Metab. *26*, 407–418.e403.

Everaere, L., Ait-Yahia, S., Molendi-Coste, O., Vorng, H., Quemener, S., LeVu, P., Fleury, S., Bouchaert, E., Fan, Y., Duez, C., et al. (2016). Innate lymphoid cells contribute to allergic airway disease exacerbation by obesity. J. Allergy Clin. Immunol. *138*, 1309–1318.e1311.

Fanta, C.H. (2009). Asthma. N. Engl. J. Med. *360*, 1002–1014.

Fumagalli, M., Moltke, I., Grarup, N., Racimo, F., Bjerregaard, P., Jørgensen, M.E., Korneliussen, T.S., Gerbault, P., Skotte, L., Linneberg, A., et al. (2015). Greenlandic Inuit show genetic signatures of diet and climate adaptation. Science *349*, 1343–1347.

Futatsugi, K., Kung, D.W., Orr, S.T., Cabral, S., Hepworth, D., Aspnes, G., Bader, S., Bian, J., Boehm, M., Carpino, P.A., et al. (2015). Discovery and optimization of imidazopyridine-based inhibitors of diacylglycerol acyltransferase 2 (DGAT2). J. Med. Chem. *58*, 7173–7185.

Gaebler, A., Penno, A., Kuerschner, L., and Thiele, C. (2016). A highly sensitive protocol for microscopy of alkyne lipids and fluorescently tagged or immunostained proteins. J. Lipid Res. *57*, 1934–1947.

Garbarino, J., Padamsee, M., Wilcox, L., Oelkers, P.M., D'Ambrosio, D., Ruggles, K.V., Ramsey, N., Jabado, O., Turkish, A., and Sturley, S.L. (2009). Sterol and diacylglycerol acyltransferase deficiency triggers fatty acid-mediated cell death. J. Biol. Chem. *284*, 30994–31005.

Halim, T.Y., Krauss, R.H., Sun, A.C., and Takei, F. (2012). Lung natural helper cells are a critical source of Th2 cell-type cytokines in protease allergen-induced airway inflammation. Immunity *36*, 451–463.

Hammad, H., and Lambrecht, B.N. (2015). Barrier epithelial cells and the control of type 2 immunity. Immunity *43*, 29–40.

Herms, A., Bosch, M., Ariotti, N., Reddy, B.J., Fajardo, A., Fernández-Vidal, A., Alvarez-Guaita, A., Fernández-Rojo, M.A., Rentero, C., Tebar, F., et al. (2013). Cell-to-cell heterogeneity in lipid droplets suggests a mechanism to reduce lipotoxicity. Curr. Biol. *23*, 1489–1496.

Holgate, S.T., and Polosa, R. (2008). Treatment strategies for allergy and asthma. Nat. Rev. Immunol. *8*, 218–230.

Huang, J.T., Welch, J.S., Ricote, M., Binder, C.J., Willson, T.M., Kelly, C., Witztum, J.L., Funk, C.D., Conrad, D., and Glass, C.K. (1999). Interleukin-4-dependent production of PPAR-gamma ligands in macrophages by 12/15-lipoxygenase. Nature *400*, 378–382.

Iturralde, M., Gamen, S., Pardo, J., Bosque, A., Piñeiro, A., Alava, M.A., Naval, J., and Anel, A. (2003). Saturated free fatty acid release and intracellular ceramide generation during apoptosis induction are closely related processes. Biochim. Biophys. Acta *1634*, 40–51.

Kassan, A., Herms, A., Fernández-Vidal, A., Bosch, M., Schieber, N.L., Reddy, B.J., Fajardo, A., Gelabert-Baldrich, M., Tebar, F., Enrich, C., et al. (2013). Acyl-CoA synthetase 3 promotes lipid droplet biogenesis in ER microdomains. J. Cell Biol. *203*, 985–1001.

Kennedy, A.R., Pissios, P., Otu, H., Roberson, R., Xue, B., Asakura, K., Furukawa, N., Marino, F.E., Liu, F.F., Kahn, B.B., et al. (2007). A high-fat, ketogenic diet induces a unique metabolic state in mice. Am. J. Physiol. Endocrinol. Metab. *292*, E1724–E1739.

King, A.J., Segreti, J.A., Larson, K.J., Souers, A.J., Kym, P.R., Reilly, R.M., Collins, C.A., Voorbach, M.J., Zhao, G., Mittelstadt, S.W., and Cox, B.F. (2010). In vivo efficacy of acyl CoA: diacylglycerol acyltransferase (DGAT) 1 inhibition in rodent models of postprandial hyperlipidemia. Eur. J. Pharmacol. *637*, 155–161.

Listenberger, L.L., Han, X., Lewis, S.E., Cases, S., Farese, R.V., Jr., Ory, D.S., and Schaffer, J.E. (2003). Triglyceride accumulation protects against fatty acid-induced lipotoxicity. Proc. Natl. Acad. Sci. USA *100*, 3077–3082.

Lloyd, C.M., and Hessel, E.M. (2010). Functions of T cells in asthma: more than just T(H)2 cells. Nat. Rev. Immunol. *10*, 838–848.

Lutas, A., and Yellen, G. (2013). The ketogenic diet: metabolic influences on brain excitability and epilepsy. Trends Neurosci. *36*, 32–40.

Marcelin, G., and Chua, S., Jr. (2010). Contributions of adipocyte lipid metabolism to body fat content and implications for the treatment of obesity. Curr. Opin. Pharmacol. *10*, 588–593.

McKenzie, A.N.J., Spits, H., and Eberl, G. (2014). Innate lymphoid cells in inflammation and immunity. Immunity *41*, 366–374.

Monticelli, L.A., Buck, M.D., Flamar, A.L., Saenz, S.A., Tait Wojno, E.D., Yudanin, N.A., Osborne, L.C., Hepworth, M.R., Tran, S.V., Rodewald, H.R., et al. (2016). Arginase 1 is an innate lymphoid-cell-intrinsic metabolic checkpoint controlling type 2 inflammation. Nat. Immunol. *17*, 656–665.

Neal, E.G., Chaffe, H., Schwartz, R.H., Lawson, M.S., Edwards, N., Fitzsimmons, G., Whitney, A., and Cross, J.H. (2009). A randomized trial of classical and medium-chain triglyceride ketogenic diets in the treatment of childhood epilepsy. Epilepsia *50*, 1109–1117.

Nguyen, T.B., Louie, S.M., Daniele, J.R., Tran, Q., Dillin, A., Zoncu, R., Nomura, D.K., and Olzmann, J.A. (2017). DGAT1-dependent lipid droplet biogenesis protects mitochondrial function during starvation-induced autophagy. Dev. Cell *42*, 9–21.e25.

Novey, H.S., Marchioli, L.E., Sokol, W.N., and Wells, I.D. (1979). Papain-induced asthma—physiological and immunological features. J. Allergy Clin. Immunol. *63*, 98–103.

Nussbaum, J.C., Van Dyken, S.J., von Moltke, J., Cheng, L.E., Mohapatra, A., Molofsky, A.B., Thornton, E.E., Krummel, M.F., Chawla, A., Liang, H.E., and Locksley, R.M. (2013). Type 2 innate lymphoid cells control eosinophil homeostasis. Nature *502*, 245–248.

Oboki, K., Ohno, T., Kajiwara, N., Arae, K., Morita, H., Ishii, A., Nambu, A., Abe, T., Kiyonari, H., Matsumoto, K., et al. (2010). IL-33 is a crucial amplifier of innate rather than acquired immunity. Proc. Natl. Acad. Sci. USA *107*, 18581–18586.

Pearce, E.L., and Pearce, E.J. (2013). Metabolic pathways in immune cell activation and quiescence. Immunity *38*, 633–643.

Pearce, E.L., Poffenberger, M.C., Chang, C.H., and Jones, R.G. (2013). Fueling immunity: insights into metabolism and lymphocyte function. Science *342*, 1242454.

Pelgrom, L.R., and Everts, B. (2017). Metabolic control of type 2 immunity. Eur. J. Immunol. *47*, 1266–1275.

Platts-Mills, T.A. (2015). The allergy epidemics: 1870-2010. J. Allergy Clin. Immunol. *136*, 3–13.

Powell, J.D., and Delgoffe, G.M. (2010). The mammalian target of rapamycin: linking T cell differentiation, function, and metabolism. Immunity *33*, 301–311.

Rambold, A.S., Cohen, S., and Lippincott-Schwartz, J. (2015). Fatty acid trafficking in starved cells: regulation by lipid droplet lipolysis, autophagy, and mitochondrial fusion dynamics. Dev. Cell *32*, 678–692.

Robinette, M.L., Fuchs, A., Cortez, V.S., Lee, J.S., Wang, Y., Durum, S.K., Gilfillan, S., and Colonna, M.; Immunological Genome Consortium (2015). Transcriptional programs define molecular characteristics of innate lymphoid cell classes and subsets. Nat. Immunol. *16*, 306–317.

Robinson, D.S., Hamid, Q., Ying, S., Tsicopoulos, A., Barkans, J., Bentley, A.M., Corrigan, C., Durham, S.R., and Kay, A.B. (1992). Predominant TH2-like bronchoalveolar T-lymphocyte population in atopic asthma. N. Engl. J. Med. *326*, 298–304.

Salmond, R.J., Mirchandani, A.S., Besnard, A.G., Bain, C.C., Thomson, N.C., and Liew, F.Y. (2012). IL-33 induces innate lymphoid cell-mediated airway inflammation by activating mammalian target of rapamycin. J Allergy Clin. Immunol. *130*, 1159–1166.e1156.

Spits, H., Artis, D., Colonna, M., Diefenbach, A., Di Santo, J.P., Eberl, G., Koyasu, S., Locksley, R.M., McKenzie, A.N., Mebius, R.E., et al. (2013). Innate lymphoid cells—a proposal for uniform nomenclature. Nat. Rev. Immunol. *13*, 145–149.

Spits, H., and Di Santo, J.P. (2011). The expanding family of innate lymphoid cells: regulators and effectors of immunity and tissue remodeling. Nat. Immunol. *12*, 21–27.

Thiele, C., Wunderling, K., and Leyendecker, P. (2019). Multiplexed and single cell tracing of lipid metabolism. Nat. Methods *16*, 1123–1130.

Townsend, M.J., Fallon, P.G., Matthews, D.J., Jolin, H.E., and McKenzie, A.N. (2000). T1/ST2-deficient mice demonstrate the importance of T1/ST2 in developing primary T helper cell type 2 responses. J. Exp. Med. *191*, 1069–1076.

Unger, R.H., Clark, G.O., Scherer, P.E., and Orci, L. (2010). Lipid homeostasis, lipotoxicity and the metabolic syndrome. Biochim. Biophys. Acta *1801*, 209–214.

Vivier, E., Artis, D., Colonna, M., Diefenbach, A., Di Santo, J.P., Eberl, G., Koyasu, S., Locksley, R.M., McKenzie, A.N.J., Mebius, R.E., et al. (2018). Innate lymphoid cells: 10 years on. Cell *174*, 1054–1066.

Wilhelm, C., Hirota, K., Stieglitz, B., Van Snick, J., Tolaini, M., Lahl, K., Sparwasser, T., Helmby, H., and Stockinger, B. (2011). An IL-9 fate reporter demonstrates the induction of an innate IL-9 response in lung inflammation. Nat. Immunol. *12*, 1071–1077.

Wilhelm, C., Harrison, O.J., Schmitt, V., Pelletier, M., Spencer, S.P., Urban, J.F., Jr., Ploch, M., Ramalingam, T.R., Siegel, R.M., and Belkaid, Y. (2016). Critical role of fatty acid metabolism in ILC2-mediated barrier protection during malnutrition and helminth infection. J. Exp. Med. *213*, 1409–1418.

Yamaguchi, M., Samuchiwal, S.K., Quehenberger, O., Boyce, J.A., and Balestrieri, B. (2018). Macrophages regulate lung ILC2 activation via Pla2g5-dependent mechanisms. Mucosal Immunol. *11*, 615–626.

Yao, C.H., Fowle-Grider, R., Mahieu, N.G., Liu, G.Y., Chen, Y.J., Wang, R., Singh, M., Potter, G.S., Gross, R.W., Schaefer, J., et al. (2016). Exogenous fatty acids are the preferred source of membrane lipids in proliferating fibroblasts. Cell Chem. Biol. *23*, 483–493.

STAR★METHODS

KEY RESOURCES TABLE

REAGENT or RESOURCE	SOURCE	IDENTIFIER
Antibodies		
CD11b Mouse/human	Biolegend	Cat# 101204; RRID:AB_312787
CD11c Mouse	eBioscience	Cat# 25-0114-82; RRID:AB_469590
CD25 Mouse	eBioscience	Cat# 45-0251-82; RRID:AB_914324
CD4 Mouse	Biolegend	Cat# 100512; RRID:AB_312715
CD45 Mouse	Biolegend	Cat# 103116; RRID:AB_312981
CD90.2 Mouse	Biolegend	Cat# 140310; RRID:AB_10643586
GATA3 Mouse	BD	Cat# 560078; RRID:AB_1645317
IL-13 Mouse	eBioscience	Cat# 53-7133-82; RRID:AB_2016708
IL-33R Mouse	Biolegend	Cat# 145304; RRID:AB_2561915
IL-5 Mouse/human	Biolegend	Cat# 504304; RRID:AB_315328
Ki67 Mouse	eBioscience	Cat# 25-5698-82; RRID:AB_11220070
Ly6G Mouse	Biolegend	Cat# 127614; RRID:AB_2227348
MHC-II Mouse	Biolegend	Cat# 107622; RRID:AB_493727
Sca-1 Mouse	eBioscience	Cat# 56-5981-82; RRID:AB_657836
Streptavidin	Biolegend	Cat# 405225
TCRß Mouse	eBioscience	Cat# 45-5961-82; RRID:AB_925763
Siglec F Mouse	BD Biosciences	Cat# 562680; RRID:AB_2687570
CD3 Mouse	Biolegend	Cat# 100304; RRID:AB_312669
NK1.1 Mouse	Biolegend	Cat# 108704; RRID:AB_313391
Gr-1 Mouse	Biolegend	Cat# 108404; RRID:AB_313369
DX5 Mouse	Biolegend	Cat# 108904; RRID:AB_313411
CD19 Mouse	Biolegend	Cat# 115504; RRID:AB_313639
Ter119 Mouse	Biolegend	Cat# 116204; RRID:AB_313705
CD11b Mouse/human	Biolegend	Cat# 101204; RRID:AB_312787
CD11c Mouse	Biolegend	Cat# 117304; RRID:AB_313773
PPARg Mouse	Thermo Fisher Scientific	Cat# MA514889; RRID:AB_10985650
PLIN2(ADFP) Mouse	Abcam	Cat# ab108323; RRID:AB_10863476
Phospho-mTOR Mouse	eBioscience	Cat# 12-9718-42; RRID:AB_2572724
Phospho-S6 Mouse	eBioscience	Cat# 25-9007-42; RRID:AB_2637099
Alexa Fluor 488 Goat anti-Rabbit IgG	Thermo Fisher Scientific	Cat# A-11008; RRID:AB_143165
Alexa Fluor 647 Goat anti-Rabbit IgG	Thermo Fisher Scientific	Cat# A-21244; RRID:AB_2535812
Alexa Fluor 700 Goat anti-Rabbit IgG	Thermo Fisher Scientific	Cat# A-21038; RRID:AB_2535709
Chemicals, Peptides, and Recombinant Proteins		
2-NBDG	Cayman	Cat# 11046
2-Propanol > 99.8% Rotipuran 2.5 Liter	Roth	Cat# 9866.2
Alternaria alternata	Greer	Cat# XPMID3A25
BODIPY 493/503	Thermo Fisher Scientific	Cat# D3922
BODIPY FL C16	Thermo Fisher Scientific	Cat# D3821
BODIPY FL C12	Thermo Fisher Scientific	Cat# D3822
Chloroform	Amresco	Cat# 0757-500mL
DAPI	Roth	Cat#6335.1
DMSO - Dimethyl sulfoxide	Biozol	Cat# EMR385250
Ethanol ≥ 99.5%, Ph.Eur., reinst	Roth	Cat# 5054.4
Fatty Acid Supplement	Sigma Aldrich	Cat# F7050

(*Continued on next page*)

Continued

REAGENT or RESOURCE	SOURCE	IDENTIFIER
Fetal Bovine Serum	Thermo Fisher Scientific	Cat# 10270106
FoxP3/Transcription Staining Set	Thermo Fisher Scientific	Cat# 00-5523-00
Golgi Plug	BD Bioscience	Cat# 51-2301KZ
HEPES Buffer 1M	PAN Biotech	Cat# P05-01100
Tween	Sigma	Cat# P1379
IL-2	Biolegend	Cat# 575404
IL-25	Biolegend	Cat# 587304
IL-33	Biolegend	Cat# 580502
IL-7	Biolegend	Cat# 577802
TSLP	R&D Systems	Cat# 555-TS/CF
Ionomycin	Sigma	Cat# I0634-1MG
L-Glutamine (200 mM)	Thermo Fisher Scientific	Cat# A2916801
Liberase TL Research Grade	Sigma	Cat# 5401020001
MojoSort Streptavidin Nanobeads	Biolegend	Cat# 480016
Papain	Merck	Cat# 5125
Penicillin-Streptomycin	Thermo Fisher Scientific	Cat# 15140122
Percoll	GE Healthcare	Cat# 17-0891-01
Phorbol-12-myristate-13-acetate	Biomol	Cat# LKT-P2857.5
RPMI Medium 1640	Thermo Fisher Scientific	Cat# 21875-091
Sodium pyruvate	Sigma	Cat# P2256-25G
β-Mercaptoethanol	PAN Biotech	Cat# P07-05020
Trizol	Thermo Fisher Scientific	Cat# 15596018
A922500	Targetmol	Cat# T6365
GW9662	Cayman Chemicals	Cat# 70785
Linoleic oleic acid BSA	Sigma	Cat# L9655
Palmitic acid	Cayman Chemicals	Cat# 10006627
Palmitic acid click	Prof. Dr. Christoph Thiele	Cat# N.A.
PF06424439	Tocris	Cat# 6348
ProLong Diamond Antifade Mountant	Thermo Fisher Scientific	Cat# P36970
Rapamycin	Enzo	Cat# BML-A275
TAT-cre Recombinase	Merck	Cat# SCR508
Critical Commercial Assays		
FoxP3/Transcription staining set	Thermo Fisher Scientific	Cat# 00-5523-00
Free Fatty Acid Fluorometric Assay Kit	Cayman	Cat# 700310
Zombie UV Viability Kit	Biolegend	Cat# 423108
Glucose-Glo Assay	Promega	Cat# J6021
Legendplex	Biolegend	Cat# 740446
Click-iT Lipid Peroxidation Imaging Kit – Alexa Fluor 488	Thermo Fisher Scientific	Cat# C10446
Experimental Models: Organisms/Strains		
Mouse: C57BL/6N	Charles River	N/A
Mouse: *Il1rl1*$^{-/-}$	MRC-LMB (A. McKenzie)	N/A
Mouse: B6. Red5$^{cre/+}$*Dgat1*$^{fl/fl}$	R. Locksley (Red5) and Charles River (*Dgat1*$^{fl/fl}$)	N/A
Mouse: B6. Red5$^{cre/+}$*Pparg*$^{fl/fl}$	R. Locksley (Red5) and Charles River (*Pparg*$^{fl/fl}$)	N/A
Mouse: Red5 (*Il5*$^{tm1.1(icre)Lky}$)	R. Locksley	N/A
Mouse: *Dgat1*$^{fl/fl}$	Charles River	N/A
Mouse: *Pparg*$^{fl/fl}$	Charles River	N/A

(*Continued on next page*)

Continued

REAGENT or RESOURCE	SOURCE	IDENTIFIER
Oligonucleotides		
Acaca	IDT	Mm. PT. 58.12492865. Exon 28-29
Acly	IDT	Mm. PT. 58.33265203. Exon 16-17
Acox1	IDT	Mm. PT. 58.46346115. Exon 7-8
Cpt1a	IDT	Mm. PT. 58.10147164. Exon 12-13
Dgat1	IDT	Mm. PT. 58.32759507. Exon 2-4
Dgat2	IDT	Mm. PT. 58.28629966. Exon 7-8
Fasn	IDT	Mm. PT. 58.14276063. Exon 1-2
Got1	IDT	Mm. PT. 58.10848799. Exon 2-3
Hk1	IDT	Mm. PT. 58.9947184. Exon 15-16
Hmgcs1	IDT	Mm. PT. 58.11355121. Exon 5-6
Hprt	IDT	Mm. PT. 39a.22214828. Exon 6-7
Ldha	IDT	Mm. PT. 58.29860774. Exon 3-4
Pkm	IDT	Mm. PT. 58.6642152. Exon 3-4
Ppara	IDT	MM. PT. 58.9374886. Exon 8-9
Pparg	IDT	Mm. PT. 58.31161924. Exon 4-5
Slc27a6	IDT	Mm. PT. 58.9548097. Exon 1-2
Srebf1	IDT	Mm. PT. 58.7535355. Exon 6-7
Ucp2	IDT	Mm. PT. 58.11226903. Exon 2-3
Il-5	IDT	Mm. PT. 58.41498972. Exon 1-3
Il-13	Thermo Fisher Scientific	Mm00434204_m1
Software and Algorithms		
Adobe Illustrator CC	Adobe	https://www.adobe.com/de/products/illustrator.html
Prism Graphpad 6	GraphPad Software	https://www.graphpad.com/scientific-software/prism/
QuantStudio Design & Analysis Software	Applied Biosystems by Thermo Fischer Scientific	https://www.thermofisher.com/de/de/home/technical-resources/software-downloads/ab-quantstudio-3-and-5-real-time-pcr-system.html
Gen5 Microplate reader and imager software	BioTek	https://www.biotek.com/products/software-robotics-software/gen5-microplate-reader-and-imager-software/
Legenplex Data Analysis Software	Biolegend	https://www.biolegend.com/legendplex
FlowJo V10	FlowJO	https://www.flowjo.com/solutions/flowjo/downloads/
FIJI Software	National Institutes of Health	http://fiji.sc/
IDEAS software	Luminex	https://www.luminexcorp.com/imaging-flow-cytometry-support/#overview
Other		
ClustVis	ClustVis	https://biit.cs.ut.ee/clustvis/

LEAD CONTACT AND MATERIALS AVAILABILITY

Further information and requests for resources and reagents should be directed to and will be fulfilled by the Lead Contact, Christoph Wilhelm (christoph.wilhelm@uni-bonn.de).

EXPERIMENTAL MODEL AND SUBJECT DETAILS

Animals

C57BL/6 (WT) were bred in-house or purchased from Charles River labs and maintained at in-house facilities. *Il1rl1*$^{-/-}$ mice on a C57BL/6 background (kindly provided by Dr. Andrew McKenzie, MRC Laboratory of Molecular Biology, Cambridge) were bred

in-house. *Red5* animals (kindly provided by Dr. Richard Locksley, University of California, San Francisco) were crossed to *Dgat1*$^{fl/fl}$ and *Pparg* $^{fl/fl}$ (both purchased from Jackson Laboratory) and maintained at in-house facilities. All mice were kept under specified pathogen free (SPF) conditions. All procedures were performed according to ethical protocols approved by the local and regional ethics committees. All mice used were between 6-10 weeks of age.

Induction of papain and Alternaria alternata

C57BL/6 mice were anaesthetized with isoflurane and exposed intranasally to 10 μg papain (Callbiochem) or 10 μg of total protein from *Alternaria alternata* extract (Greer) in 50 μl PBS on days 0, 3, 6. Seven days later mice were re-challenged intranasally with 10 μg papain or *Alternaria* allergen in PBS. 18 h after the last allergen challenge lung homogenate was obtained by meshing diced lung fragments trough a 40 μm cell strainer, and the cell-free supernatant was stored at −80°C for cytokine analysis.

Intranasal IL-25, IL-33, and TSLP administration

WT B6 mice were intranasally challenged with 100 ng recombinant mouse IL-25, IL-33, or TSLP (all from Biolegend) in 50 μl PBS on days 0, 1, and 3. Control animals received PBS only. Mice were euthanized 18 h after the challenge and lung cells were isolated for analysis.

METHOD DETAILS

Cell isolation from tissues and flow cytometry

Lung tissues were diced and digested with 0.25 mg/ml Liberase TL (Roche) and 1 mg/ml DNase I (Sigma) at 37°C for 1 h. Isolated lung cells were further purified using a 37.5% Percoll gradient, followed by lysis of red blood cells with Ammonium-Chloride-Potassium (ACK) lysing buffer. Single-cell suspensions were stained with anti-CD16/32 (BioXcell) and with fluorochrome-conjugated antibodies against any combination of the following surface antigens: CD3, CD11b, CD11c, DX5, CD19, CD45, Ter119, NK1.1, Gr-1, CD45, Thy1.2, and ST2. DAPI or fixable Zombie UV dye (Biolegend) were used to exclude dead cells. For examination of transcription factors and cellular proliferation, cells were subsequently treated with the Foxp3 fixation/permeabilization kit (eBioscience) in accordance with the manufacturer's instructions and stained for 30 min on ice with fluorochrome-conjugated antibodies against GATA3 and Ki67.

Re-stimulation of cells for intracellular cytokine staining

Cells isolated from lung tissues were stimulated for 3 h with Phorbol 12,13-dibutyrate (0.5 μg/ml) (PdBU; Biomol) and ionomycin (0.5 μg/ml) (Sigma) in the presence of brefeldin A (1 μg/ml) (GolgiPlug, BD Biosciences). Stimulated cells were stained for surface markers, fixed with 3.7% formaldehyde (Sigma), followed by fixation with Foxp3 fixation/permeabilization kit (eBioscience) in accordance with the manufacturer's instructions, and stained with antibodies against GATA3, IL-5, and IL-13.

Fluorescence-activated cell sorting, purification, and *in vitro* culture of ILC

ILC2 were sorted by flow cytometry from total lung cells isolated from naive or papain-challenged mice based on the absence of lineage markers (CD3, CD11b, CD11c, CD49b, CD19, Ter119, NK1.1, and Gr-1) but with expression of Thy1.2, CD45, and ST2. Purification of lung ILC2 was performed using a negative selection strategy. Total lung cells were stained with a combination of monoclonal antibodies against CD3, CD11b, CD11c, CD49b, CD19, Ter119, NK1.1, and Gr-1 coupled to biotin followed by incubation with Streptavidin-coupled magnetic microbeads (Biolegend) and negative selection on magnetic columns (Miltenyi). Purified or sort-purified ILC2 ($5x10^3$ cells/well) were cultured in 50 μL RPMI 1640 supplemented with 3% FBS, penicillin, streptomycin, HEPES, glutamine, pyruvate, nonessential amino acids, 50mM β-mercaptoethanol (Complete Media), and IL-2 (10 ng/ml, Biolegend) or IL-7 (10 ng/ml, Biolegend) for 3 days. In some experiments, a combination of IL-2 and IL-25, IL-33, or TSLP (10 ng/ml each) was added to the culture medium. To assess the effects of DGAT1 and PPARγ, purified ILC2 were cultured with IL-2 in the presence of increasing amounts (10 μM – 40 μM) of DGAT1 inhibitor (A922500, Targetmol) or PPARγ inhibitor (40 μM, GW9662, Cayman Chemicals). To test the functionality of FFA, ILC2 were cultured in the presence of IL-2 and a mixture of linoleic acid-BSA and oleic acid-BSA (Sigma) or 20 μM palmitic acid-BSA (Sigma and coupled to BSA in house) for 3 days. In some experiments, addition of FFA was probed in the presence of 20 μM A922500. To test the effects of glucose deprivation, purified ILC2 were cultured in the presence or absence of glucose and pyruvate.

Neutral lipid staining and uptake of 2-NBDG and BODIPY

Cultured ILC2 or freshly-isolated lung cells were stained with 200 ng/ml BODIPY 493/503 or 25 ng/ml BODIPY FL C_{16} (both ThermoFisher) for 30 min at 37°C in FBS free complete medium, washed, and analyzed by flow cytometry. To probe for uptake of 2-NBDG (2-deoxy-2-[(7-nitro-2,1,3-benzoxadiazol-4-yl)amino]-D-glucose), cells were incubated with 16 μg/ml 2-NBDG (Cayman) in glucose free RPMI for 15 min at 37°, washed, and analyzed by flow cytometry.

Flow cytometric determination of apoptosis (Annexin V / propidium iodide staining)

ILC2 were cultured for two days with IL-2 (10 ng/ml, Biolegend) or with IL-2 in the presence of DGAT1 inhibitor (40μM). The culture was analyzed by using annexin V/propidium iodide double staining (Biolegend), following the manufacturer's instructions.

Lipid peroxidation staining

ILC2 ($5x10^3$ cells/well) were cultured in 50 μL complete medium with IL-2 (10 ng/ml, Biolegend) or with IL-2 in the presence of DGAT1 inhibitor (40 μM). At the same time Image-iT Lipid Peroxidation Sensor BODIPY®(Thermo Fisher) was added. After two hours, cells were analyzed by flow cytometry and ratios of the signal from the 510 nm to 590 nm channels were used to quantify lipid peroxidation.

Alkyne-labeled palmitic acid uptake and staining

Cells isolated from lung tissues were incubated with 20 μM of alkyne-labeled palmitic acid (16-heptadecynoic acid, provided by Dr. Thiele) coupled with BSA for 30 min at 37°C in complete medium without FBS, washed, and stained for surface markers. After washing with FACS buffer, the cells were fixed with formaldehyde (3.7% in PBS) and permeabilized with Triton X-100 (0.5% in PBS). Subsequently, the alkyne-palmitic acid taken up by the cells was detected with the azide-based Click-iT detection kit (Life Technologies) according to the manufacturer's instructions. Before analysis, cells were intracellularly stained for GATA3 and Ki67.

Lipid tracing of alkyne-labeled palmitic acid and lipidomic analysis

ILC2 isolated from lung tissues were incubated at 37°C for 3 hours in complete medium with 3% FBS containing 10 ng/ml IL-7. Cells were washed and incubated for 24 hours with 20 μM alkyne-labeled palmitic acid (16-heptadecynoic acid, provided by Dr. Thiele) at 37°C in complete medium with 3% FBS. At the end of the incubation, cells were resuspended in 500 μl of extraction mix (490 μL MeOH/$CHCl_3$ 5:1 and 10 μL internal standard mix containing alkyne-labeled lipids) and processed for extraction and click reaction, as previously described by Thiele et al. (Thiele et al., 2019). The dissolved lipids were analyzed on a Thermo Q Exactive Plus spectrometer equipped with a standard heated electrospray ionization ion source using direct injection from a Hamilton syringe driven by a syringe pump under the control of the Tune instrument control software. Raw files were converted to .mzml files using MSconvert and analyzed using LipidXplorer for lipid species that incorporated the alkyne fatty acid

Lipid tracing of ^{13}C-labeled glucose

ILC2 isolated from lung tissues were incubated at 37°C for 3 hours in complete medium supplemented with 3% FCS and containing 10 ng/ml IL-7. Cells were washed and incubated for 24 hours with 11 mM of C^{13}-labeled glucose at 37°C in complete medium with 3% FBS and without glucose and pyruvate. At the end of the incubation, cells were resuspended in 500 μl of extraction mix (MeOH/$CHCl_3$ 5:1) and processed for extraction, as previously described (Thiele et al., 2019). The dissolved lipids were analyzed on a Thermo Q Exactive Plus spectrometer equipped with a standard heated electrospray ionization ion source using direct injection from a Hamilton syringe driven by a syringe pump under the control of the Tune instrument control software. Raw files were converted to .mzml files using MSconvert and analyzed using LipidXplorer for phosphatidylcholine species that had incorporated ^{13}C.

Metabolic assays

For real-time measurement of the oxygen consumption rate (OCR), purified ILC2 isolated from papain-challenged mice were cultured for 2 h with a mixture of 2 μM linoleic acid-BSA and oleic acid-BSA (Sigma) and 10 μM palmitic acid-BSA (Sigma and coupled to BSA in house) in complete media supplemented with 10 ng/ml IL-2 (Biolegend) without FBS. Cells were washed with assay medium supplemented with 10 mM glucose, 1 mM pyruvate, and 2 mM glutamine and analyzed with an XF-96 Extracellular Flux Analyzer (Agilent). For assessment of glucose metabolism, ILC2 were cultured for 2 h with or without 10 mM glucose in complete media supplemented with 10 ng/ml IL-2 (Biolegend) and 3% FBS. Cells were washed with assay medium supplemented with 10 mM glucose (or without), 1 mM pyruvate, and 2 mM glutamine and analyzed with an XF-96 Extracellular Flux Analyzer (Agilent). Three or more consecutive measurements were obtained under basal conditions followed by the addition of 1 μM oligomycin, which inhibits the mitochondrial ATP synthase; 1.5 μM FCCP (Carbonyl cyanide 4-(trifluoromethoxy)phenylhydrazone), which uncouples ATP synthesis from oxygen consumption, and a combination of 100 nM rotenone plus 0.5 μM antimycin A, which inhibit the electron transport chain by blocking complex I and III, respectively. All chemicals used for these assays were obtained from Sigma-Aldrich. Spare respiratory capacity (SRC) is calculated as the difference between basal OCR and the maximal OCR after the addition of FCCP.

In vitro TAT-Cre treatment of ILC2

ILC2 were purified from the lungs of papain treated mice and incubated at 37°C for 2 hours in complete medium without FBS containing 10 ng/ml IL-7 and 4 μM TAT-Cre recombinase (EMD-Millipore). Cells were washed 2 times with PBS and incubated at 37°C for 3 days in complete medium supplemented with 3% FBS and containing 10 ng/ml IL-2. Subsequently, cells were stained and analyzed by flow cytometry or processed for qPCR analysis.

Imaging flow cytometry

ILC2 were cultured overnight in complete medium supplemented with 3% FBS and containing 10 ng/ml IL-2. Cells were washed and stained with BODIPY FL C_{12} (Thermo Fisher) at a concentration of 200 ng/ml for 30 min at 37°C. Cells were washed with FACS buffer, stained for surface markers (CD45, Thy1.2, and IL33R) and fixed using the Foxp3 fixation/permeabilization kit (eBioscience) in accordance with the manufacturer's instructions. After fixation, cells were stained for 40 min on ice with an unconjugated primary rabbit antibody against PLIN2, followed by staining with a fluorescently-labeled secondary anti-rabbit antibody. Samples were run on an AMNIS ImageStream X MarkII imaging cytometer. Data acquisition was done using the INSPIRE software (Amnis EMD-Millipore) and the data analysis was performed using the IDEAS software (Amnis EMD-Millipore).

In vivo inhibitor treatment

To block the activity of DGAT1 or PPARγ, 30 mg/kg of DGAT1 inhibitor (A922500, Targetmol) or 1 mg/kg of PPARγ inhibitor (GW9662, Cayman Chemicals) were dissolved in 30 μL DMSO (biotechnology performance-certified) and administered intraperitoneally to C57BL/6 WT mice every day for the duration of the experiment. Control mice received DMSO only.

Diet studies

Control diet AIN 93G (17.6% protein, 7.1% fat, 11% sugar) and ketogenic diet TD.130659 (15% protein, 72% fat, 2.4% sugar) were purchased from Ssniff. Mice were weaned at three weeks on ketogenic or control diets and maintained on the appropriate diet for at least 3 weeks before treatment. Mice were maintained on these experimental diets throughout the experimental study.

Antibiotic treatment

Antibiotic treatment started 4 days before the first papain treatment. Vancomycin (0.5 g/L, Cayman), Ampicillin (1 g/L, Sigma), Neomycin (1 g/L, Sigma), and Metronidazole (1 g/L, Sigma) were provided *ad libitum* in drinking water. After dissolving the antibiotics in the drinking water, the pH was adjusted to 7.4. Amphotericin b (1 g/L, Cayman) was only provided for the first four days of antibiotic treatment.

Measurement of free fatty acids, glucose, and ketone bodies

Free fatty acid and glucose concentrations in the plasma and in the lung homogenate were measured by using Free Fatty Acid Fluorometric Assay Kit (Cayman) or the Gluco-Glo kit (Promega) by following the manufacturer's instructions. Ketone concentrations were measured by using a FreeStyle Precicion Neo H instrument (Abbott).

Histology

The left lung lobe was fixed in 10% formaldehyde solution and embedded into paraffin blocks. Sections were stained with periodic acid-Schiff (PAS) stain, and airways were assessed for PAS staining as an indication of mucus-producing cells.

Confocal microscopy

For assessment of lipid-droplet formation, ILC2 were purified and stained with BODIPY 493/503 (ThermoFisher) at a concentration of 500 ng/ml in complete RPMI without FCS for 30 min at 37°C. To assess the external uptake of lipids and storage in lipid droplets, ILC2 were stained with BODIPY FL C_{12} (ThermoFisher) at a concentration of 1 μg/ml for 30 min at 37°C. Cells were then washed with FACS buffer and spun onto glass slides by using a Cytospin, followed by fixation with formaldehyde (3.7%) and two washing steps with PBS. To determine the uptake and utilization of alkyne-palmitic acid, purified ILC2 were cultured overnight in complete medium with 3% FBS containing 2 ng/ml IL-2 and 2 μM alkyne-palmitic acid coupled with BSA. Cells were washed and cultured for 24h in medium containing 2 μM glucose and 1% FCS or proceeded directly to IF staining. After incubation, cells were washed with FACS buffer and spun onto glass slides by using a Cytospin, followed by fixation with formaldehyde (3.7%), washed two times with PBS, and permeabilized with Triton X-100 (0.5% in PBS). Subsequently, the alkyne-palmitic acids taken up by the cells were detected with the azide-based Click-iT detection kit (Life Technologies) according to the manufacturer's instructions. The nuclei were counterstained with DAPI, washed once with PBS, and the coverslips were mounted onto the glass slides with Prolong™ Diamond Antifade Mountant (Life Technologies). Cells were imaged with a LEICA SP5 AOBS confocal microscope. Image analysis was performed with the FIJI software (National Institutes of Health).

Real-time PCR

RNA was extracted from purified ILC2 using Trizol (ThermoFisher Scientific) and reverse transcribed with RevertAid Kit (Thermo Fischer Scientific) according to the manufacturer's instructions. The cDNA served as a template for amplification of the genes of interest. For analysis of genes expressed by ILC2, TaqMan probes for *acc1*, *fasn*, *hmgcs1*, *srebf*, *pparα*, *pparg, cpt1, acox1, acly, dgat1, dgat2, got1, hk1, ldha,* and *pkm, il5* (IDT) and *il13* (ThermoFisher) were used and target-gene expression was calculated using the comparative method for relative quantification upon normalization to *Hprt* gene expression.

QUANTIFICATION AND STATISTICAL ANALYSIS

Data were analyzed with the Prism software (GraphPad). A two-tailed Student's t test was used for all statistical analyses: * $p \leq 0.05$, ** $p \leq 0.01$, *** $p \leq 0.001$. Statistical details are indicated in the figure legends.

Immunity, Volume *52*

Supplemental Information

Lipid-Droplet Formation Drives Pathogenic Group 2 Innate Lymphoid Cells in Airway Inflammation

Fotios Karagiannis, Schekufe Kharabi Masouleh, Klaus Wunderling, Jayagopi Surendar, Vanessa Schmitt, Alexander Kazakov, Marcel Michla, Michael Hölzel, Christoph Thiele, and Christoph Wilhelm

Figure S1

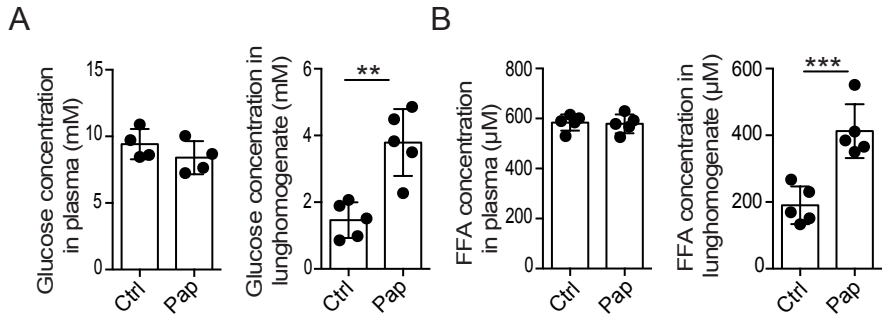

Figure S1. Related to Figure 1. Papain increases glucose and FFA concentrations in lung tissue but not in circulation. (A) Glucose concentrations in plasma and lung homogenates from PBS (Ctrl) or papain (Pap) challenged mice. **(B)** FFA concentrations in plasma and lung homogenate from PBS or papain challenged mice. Results are representative of at least three independent experiments with three to five mice in each experimental group. All graphs display means ± SEM; * $p \leq 0.05$, ** $p \leq 0.01$, *** $p \leq 0.001$.

Figure S2

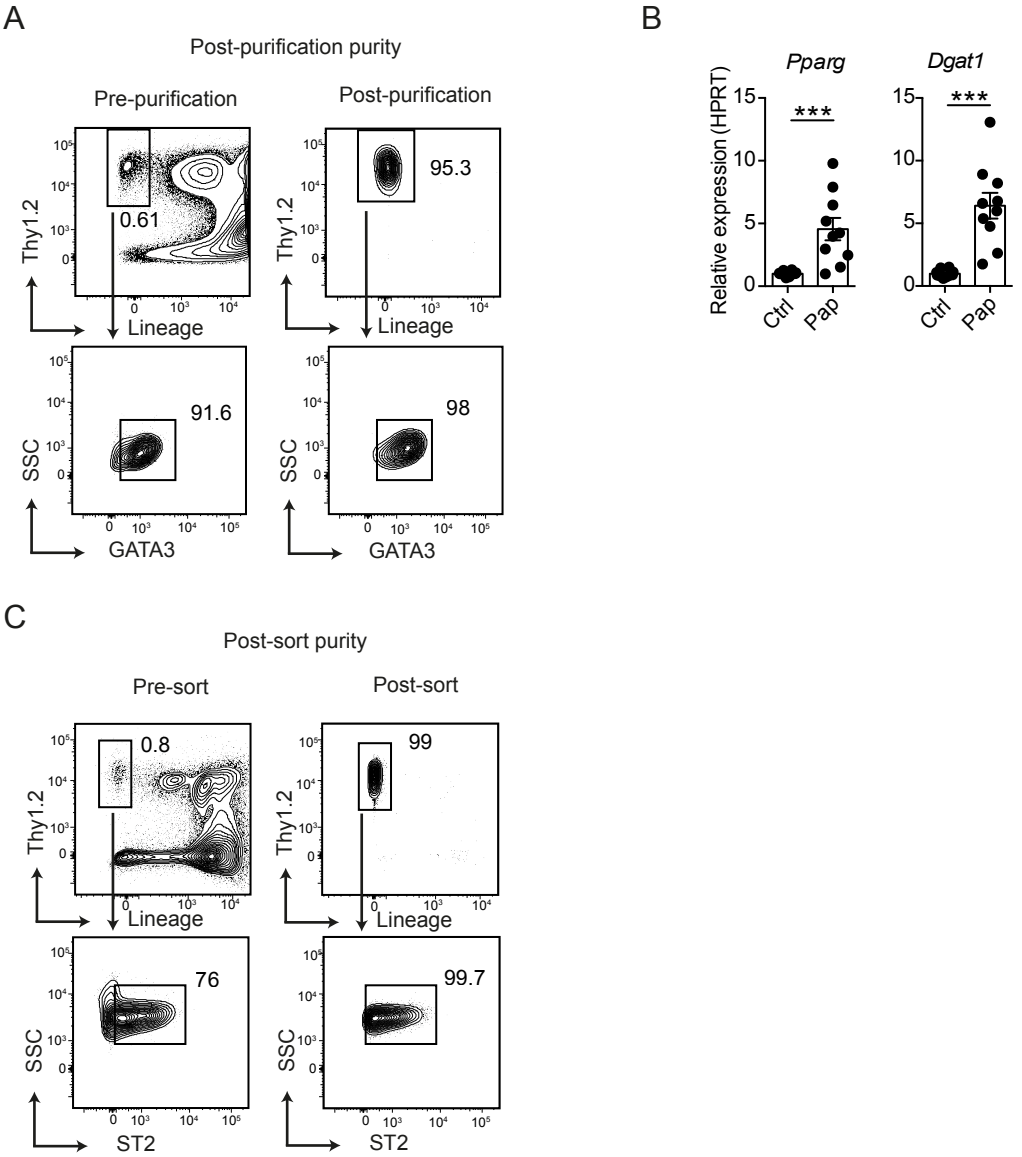

Figure S2. Related to Figure 1. Purification and sorting strategy of ILC2. (A) Total lung cells were stained with antibodies against CD3, CD11b, CD11c, CD49b, CD19, Ter119, NK1.1 and Gr-1 coupled to biotin followed by incubation with Streptavidin-coupled magnetic microbeads (Biolegend) and negative selection on magnetic columns (Miltenyi). Post-purification measurements indicating a purity greater than 98%. **(B)** RT-PCR analysis relative to *Hprt* of ILC2 isolated from papain (Pap) or PBS (Ctrl) challenged mice. **(C)** Cells were stained with lineage markers (CD3, CD11b, CD11c, CD49b, CD19, Ter119, NK1.1 and Gr-1) and Thy1.2 and gated on live and CD45+ cells. ILC2 were sorted as Thy1+, Lineage-, ST2+. Post-sort measurements indicating a purity greater than 99%. Results are representative of at least two independent experiments with three to five mice each in each experimental group (B). All graphs display means ± SEM; *** p≤0.001.

Figure S3

A

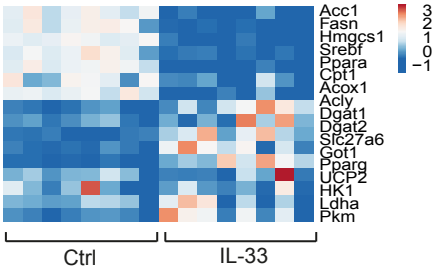

Figure S3. Related to Figure 2. Exposure to IL-33 upregulates genes involved in TAG synthesis and FA uptake. (A) RT-PCR analysis relative to *Hprt* displayed as fold change of purified lung ILC2 from IL-33 over PBS challenged animals. Results are representative of at least two independent experiments with three to five mice in each experimental group. All graphs display means ± SEM; * $p \leq 0.05$, ** $p \leq 0.01$, *** $p \leq 0.001$.

Figure S4

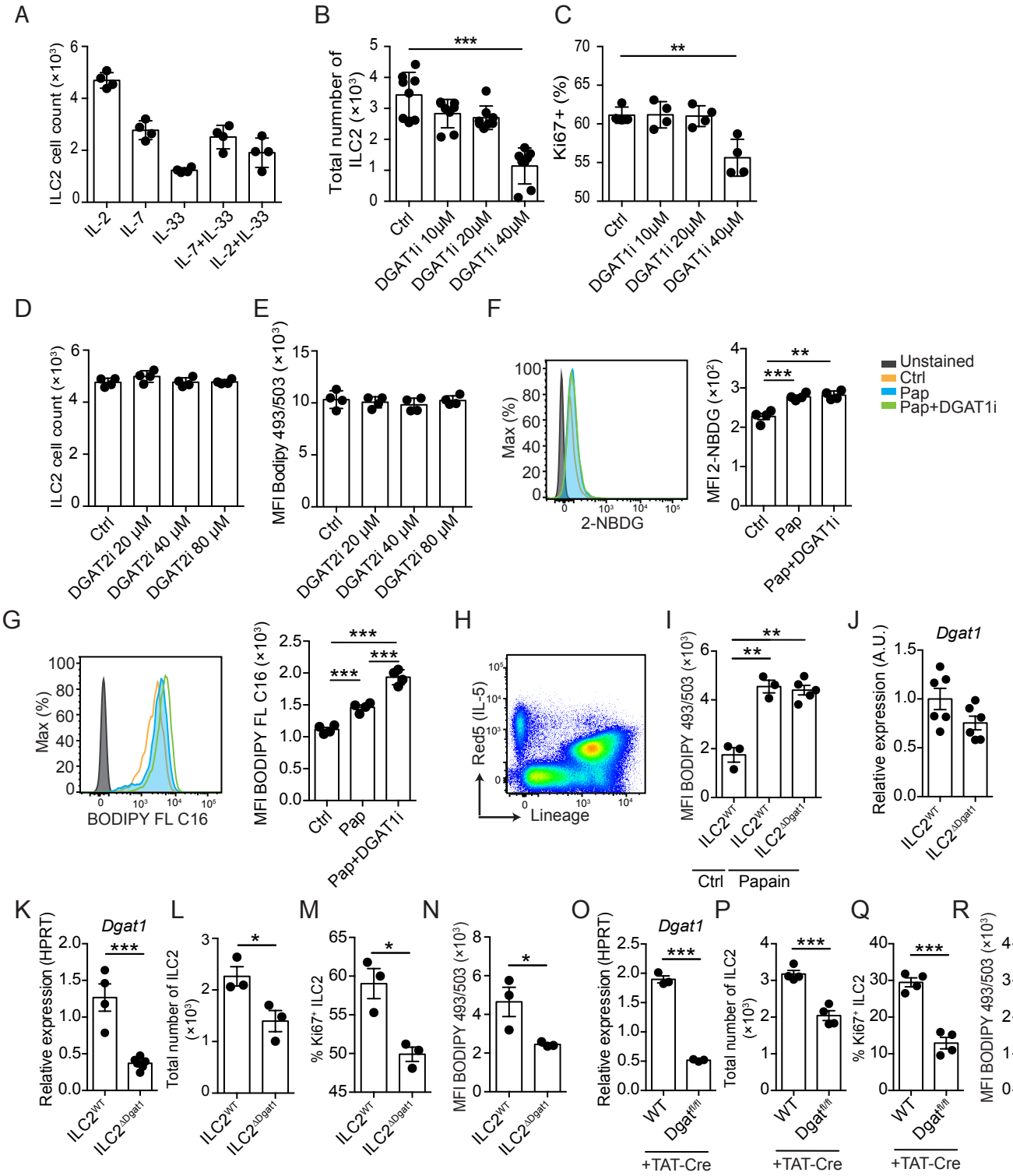

Figure S4. Related to Figure 4. DGAT1 but not DGAT2 inhibition reduces lipid droplet formation and impairs ILC2 accumulation. (A) ILC2 were purified from papain challenged C57BL/6 mice and cultured for 3 days in the presence of IL-2, IL-7, IL-33 or a combination of IL-7 and IL-33 or IL-7 and IL-2. **(B)** Total numbers of ILC2 cultured for 3 days in the presence of IL-2 with increasing concentrations of the DGAT1-Inhibitor A922500 (DGAT1i), **(C)** expression of Ki67. **(D)** Total numbers of purified ILC2 after 3 days of culture with increasing concentrations of DGAT2 inhibitor (DGAT2i) PF06424439. **(E)** BODIPY 493/503 staining of cultured ILC2. **(F)** Representative histograms and MFI values of 2-NBDG or **(G)** MFI values of BODIPY FL C16 uptake in lung ILC2 (Lin– Thy1.2+ ST2+) of ILC2 from PBS (Ctrl), papain (Pap) or papain challenged mice treated with DGAT1i (Pap+DGAT1i). **(H)** Flow cytometric analysis of cells isolated from the lung of papain challenged *ILC2^{WT}* animals at day 14. Panel represents live CD45+ cells stained with lineage (Lin) markers and assessed for RFP (Red5) expression. **(I)** BODIPY 493/503 in lung ILC2 from control (Ctrl) or papain (Pap) challenged *ILC2^{WT}* and *ILC2$^{\Delta Dgat1}$* mice. **(J)** RT-PCR analysis displayed as arbitrary units (A.U.) of ILC2 isolated from *ILC2$^{\Delta Dgat1}$* over *ILC2^{WT}* mice challenged with papain **(K)** RT-PCR analysis relative to *Hprt* of cultured ILC2, **(L)** total numbers, **(M)** percentages of Ki67+ ILC2 or **(N)** BODIPY 493/503 staining in cultured ILC2 from papain challenged *ILC2^{WT}* or *ILC2$^{\Delta Dgat1}$* mice. **(O)** RT-PCR analysis relative to *Hprt* of cultured ILC2, **(P)** total numbers of ILC2, **(Q)** percentages of Ki67+ ILC2 or **(R)** BODIPY 493/503 staining in cultured ILC2 from papain challenged *WT* or *Dgat1$^{fl/fl}$* mice treated with TAT-Cre. Results are representative of at least two independent experiments or pooled data of two experiments **(J)** with three to five mice in each experimental group. All graphs display means ± SEM; * p≤ 0.05, **p ≤ 0.01, *** p≤0.001.

Figure S5

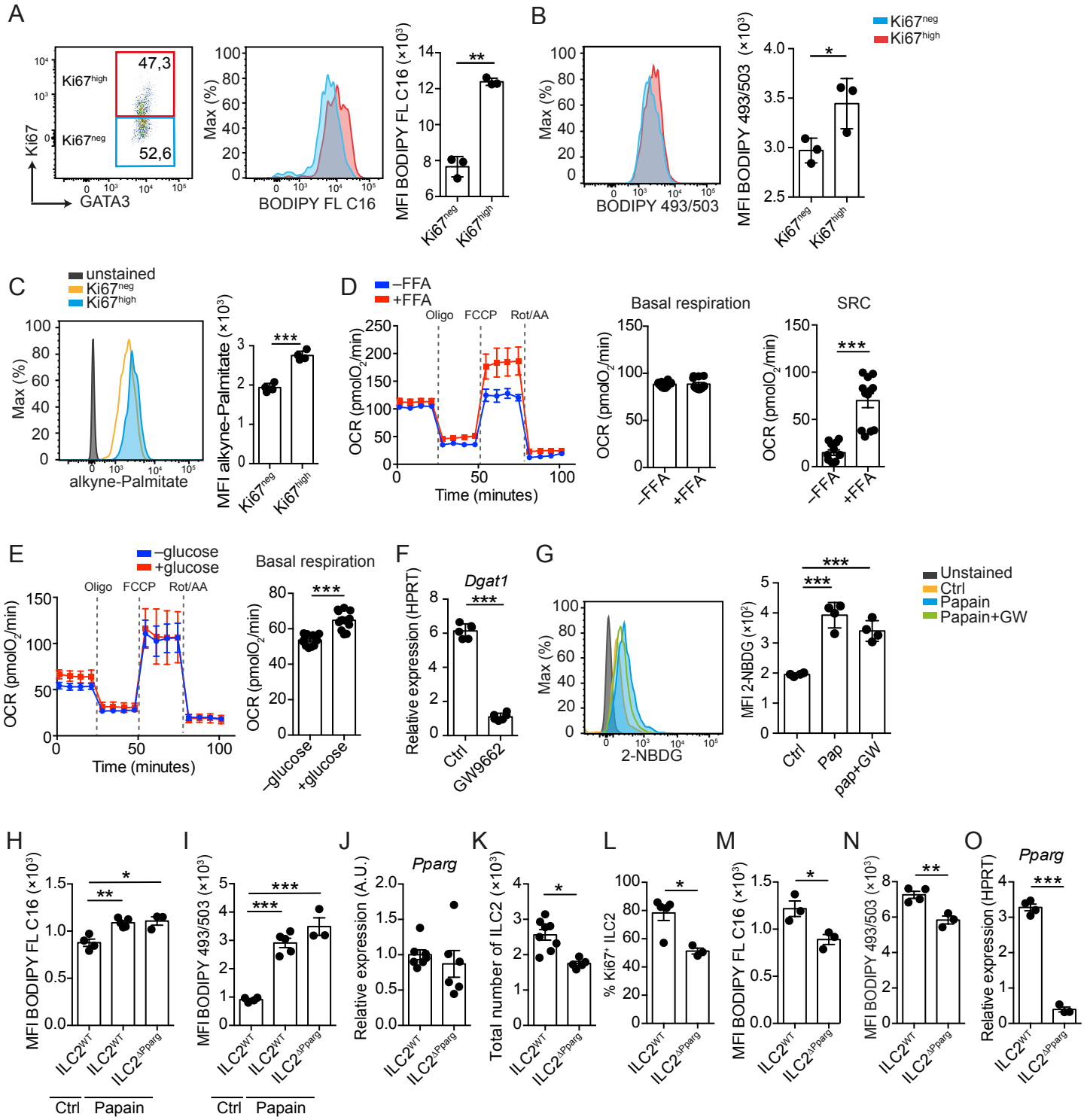

Figure S5. Related to Figure 5. Proliferating ILC2 take up more fatty acids and build up more lipid droplets compared to non proliferating ILC2. ILC2 were purified from papain challenged C57BL/6 mice and cultured for 3 days in the presence of IL-2. **(A)** Representative histograms and MFI values of BODIPY FL C16 and **(B)** BODIPY 493/503 in Ki67 positive and negative cultured ILC2. **(C)** Representative histograms and MFI values of alkyne-Palmitate in Ki67 positive and negative lung ILC2 from mice challenged with PBS or papain. (**D**) OCR, basal respiration and spare respiratory capacity (SRC) of ILC2 cultured without (–FFA) or with oleic acid-BSA and linoleic acid-BSA and palmitic acid-BSA (+FFA). (**E**) OCR and basal respiration of ILC2 cultured without (–glucose) or with glucose (+glucose). (**F**) RT-PCR analysis of ILC2 cultured in the presence or absence of the PPARγ inhibitor GW9662 relative to *Hprt*. (**G**) Representative histograms and MFI values of 2-NBDG in lung ILC2 (Lin– Thy1.2+ ST2+) from PBS (Ctrl), papain (Pap) or papain challenged mice treated with GW9662 (Pap+GW9662). (**H**) MFI values of BODIPY FL C16 and (**I**) BODIPY 493/503 in lung ILC2 from control (Ctrl) or papain (Pap) challenged *ILC2*^{WT} and *ILC2*$^{\Delta PPARg}$ mice. **(J)** RT-PCR analysis displayed as arbitrary units (A.U.) of ILC2 isolated from *ILC2*$^{\Delta Pparg}$ over *ILC2*^{WT} mice challenged with papain (**K**) Total numbers of ILC2, (**L**) percentages of Ki67^{+} ILC2, (**M**) MFI values of BODIPY FL C16 uptake, (**N**) MFI values of BODIPY 493/503 in cultured ILC2, (**O**) RT-PCR analysis relative to *Hprt* of cultured ILC2. Results are representative of at least two independent experiments or pooled data of two experiments **(J,K)** with three to five mice in each experimental group. All graphs display means ± SEM; * p≤ 0.05, **p ≤ 0.01, *** p≤0.001.

Figure S6

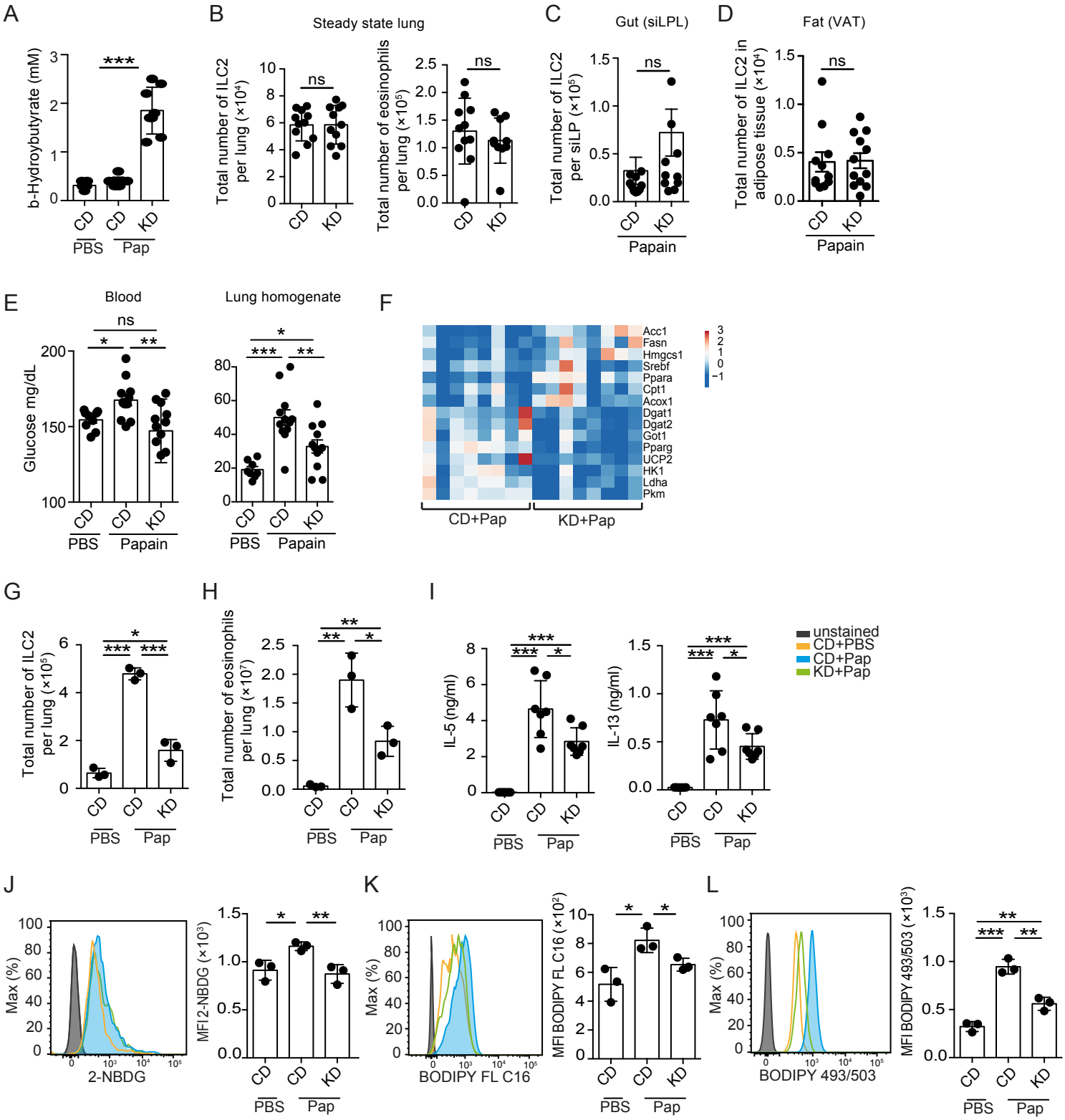

Figure S6. Related to Figure 7. Ketogenic diet does not affect ILC2 in other tissue and functions independent of the microbiota. C57BL/6 mice were placed on control diet or ketogenic diet for three weeks at the age of 3 weeks. **(A)** Ketone body concentrations in the blood of papain challenged mice on control diet and papain challenged mice on ketogenic diet. **(B)** Flow cytometric analysis of total numbers of ILC2 and eosinophils in the lung tissue of mice fed a control diet (CD) or ketogenic diet. **(C)** Total ILC2 in the small intestinal lamina propria (siLP) or **(D)** visceral adipose tissue (VAT) and **(E)** glucose concentration in the blood or lung homogenate of mice fed a control diet (CD), mice fed a control diet (CD+Pap) or ketogenic diet (KD+Pap) and challenged with papain. **(F)** RT-PCR analysis relative to HPRT displayed as fold change of ILC2 isolated from papain challenged control diet (CD) or ketogenic diet (KD) mice challenged with papain (Pap). (**G**) Flow cytometric analysis of total numbers of ILC2, (**H**) eosinophils, (**I**) total numbers of IL-5 and IL-13 producing ILC2, (**J**) representative histograms and mean fluorescence intensity (MFI) values of 2-NBDG in lung ILC2 (Lin– Thy1.2+ ST2+), (**K**) MFI values of BODIPY FL C16 uptake and (**L**) MFI values of BODIPY 493/503 analyzed in the lung tissue of PBS challenged mice fed a control diet (CD), mice fed a control diet (CD+Pap) or ketogenic diet (KD+Pap) treated with antibiotics and challenged with papain. Results are pooled data of two **(I)** or three **(B-E)** independent experiments, representative of at least two **(F-L)** or three **(A)** independent experiments with three to five mice in each experimental group. All graphs display means ± SEM; * p≤ 0.05, **p ≤ 0.01, *** p≤ 0.001.